
1 **Chemical characterization of oxygenated organic compounds**
2 **in gas-phase and particle-phase using iodide-CIMS with**
3 **FIGAERO in urban air**

4 Chenshuo Ye¹, Bin Yuan^{2,3,*}, Yi Lin^{2,3}, Zelong Wang^{2,3}, Weiwei Hu⁴, Tiange Li^{2,3}, Wei
5 Chen⁴, Caihong Wu^{2,3}, Chaomin Wang^{2,3}, Shan Huang^{2,3}, Jipeng Qi^{2,3}, Baolin Wang⁵,
6 Chen Wang⁵, Wei Song⁴, Xinming Wang⁴, E Zheng^{2,3}, Jordan E. Krechmer⁶, Penglin
7 Ye⁷, Zhanyi Zhang^{2,3}, Xuemei Wang^{2,3}, Douglas R. Worsnop⁶, Min Shao^{2,3,1}

8 ¹ College of Environmental Sciences and Engineering, Peking University, Beijing
9 100871, China

10 ² Institute for Environmental and Climate Research, Jinan University, Guangzhou
11 511443, China

12 ³ Guangdong-Hongkong-Macau Joint Laboratory of Collaborative Innovation for
13 Environmental Quality, Guangzhou 511443, China

14 ⁴ Guangzhou Institute of Geochemistry, Chinese Academy of Sciences, Guangzhou
15 511443, China

16 ⁵ School of Environmental Science and Engineering, Qilu University of Technology,
17 Jinan 250353, China

18 ⁶ Aerodyne Research, Inc., 45 Manning Rd., Billerica, MA, USA

19 ⁷ Shanghai Key Laboratory of Atmospheric Particle Pollution and Prevention (LAP³),
20 Department of Environmental Science and Engineering, Fudan University, Shanghai
21 200438, China

22 *Correspondence to: byuan@jnu.edu.cn

23

24 **Abstract**

25 The characterization of oxygenated organic compounds in urban areas remains a
26 pivotal gap in our understanding of the evolution of organic carbon under polluted
27 environments, as the atmospheric processes involving interactions between organic and
28 inorganic compounds, anthropogenic pollutants and natural emissions lead to the
29 formation of various and complex secondary products. Here, we describe
30 measurements of an iodide chemical ionization time-of-flight mass spectrometer
31 installed with a Filter Inlet for Gases and AEROSols (FIGAERO-I-CIMS) in both gas-
32 phase and particle-phase at an urban site in Guangzhou, a typical mega-city in southern
33 China, during the autumn of 2018. Abundant oxygenated organic compounds
34 containing 2-5 oxygen atoms were observed, including organic acids, multi-functional
35 organic compounds typically emitted from biomass burning, oxidation products of
36 biogenic hydrocarbons and aromatics. Photochemistry played dominant roles in the
37 formation of gaseous organic acids and isoprene-derived organic nitrates, while
38 nighttime chemistry contributed significantly to the formation of monoterpene-derived
39 organic nitrates and inorganics. Nitrogen-containing organic compounds occupied a
40 significant fraction of the total signal in both the gas and particle phases, with elevated
41 fractions at higher molecular weights. Measurements of organic compounds in particle
42 the phase by FIGAERO-I-CIMS explained $24\pm 0.8\%$ of the total organic aerosol mass
43 measured by aerosol mass spectrometer (AMS), and the fraction increased for more
44 aged organic aerosol. The systematical interpretation of mass spectra of the FIGAERO-
45 I-CIMS in the urban area of Guangzhou provides a holistic view of numerous
46 oxygenated organic compounds in the urban atmosphere, which can serve as a reference
47 for the future field measurements by FIGAERO-I-CIMS in polluted urban regions.

48

49 **1 Introduction**

50 In urban air, atmospheric chemical processes are varied and complex, as the result
51 of large emissions of both anthropogenic pollutants and biogenic volatile organic
52 compounds, associated with strong interactions with each other (He et al., 2014; Karl
53 et al., 2018; Shrivastava et al., 2019). Consequently, strong formation of secondary
54 pollutants, e.g. ozone and secondary organic aerosol (SOA), are observed in urban and
55 downwind regions (Huang et al., 2015; Zhang et al., 2014). Oxygenated organic
56 compounds are not fully accounted for in some earlier studies, which may explain some
57 of the discrepancies between observations and models for many unaddressed issues in
58 atmospheric chemistry. Oxygenated organic compounds are supposed to be the top
59 candidates for missing OH reactivity observed in various environments including
60 pristine rainforests and urbanized areas (Noelscher et al., 2016; Yang et al., 2016, 2017).
61 The photolysis of carbonyls serves as a critical radical source driving ozone formation
62 in highly polluted industrialized areas (Edwards et al., 2014; Liu et al., 2012; Xue et al.,
63 2016). Although it has been discovered a long time ago that oxygenated organic
64 compounds make up a substantial fraction of submicron aerosol mass (Kroll and
65 Seinfeld, 2008), enormous difficulty still exists in accurately predicting formation and
66 evolution of SOA (de Gouw et al., 2005; Hodzic et al., 2010; Volkamer et al., 2006).

67 One of the biggest obstacles to understanding the role of oxygenated organic
68 compounds is the characterization of these extremely complicated and diverse
69 chemicals which encompass tens of thousands of individual species spanning a wide
70 range of volatility. Chemical ionization mass spectrometry (CIMS) is a powerful
71 technique for the molecular-level characterization of oxygenated organic compounds
72 because of the following advantages (Zhao, 2018): direct measurements and fast time
73 response to capture the rapid temporal change of short-lifetime intermediates; soft
74 ionization providing chemical information on molecular level; selective ionization
75 ensuring measurements for specific classes of species. Iodide anion ionizes species
76 mainly through adduction (Iyer et al., 2016) and is used for the detection of oxygenated
77 organic compounds particularly organic compounds with 2-5 oxygen atoms (Lee et al.,

78 2014; Lopez-Hilfiker et al., 2016; Riva et al., 2019). It has been shown that I-CIMS is
79 an excellent technique to investigate oxidation processes of volatile organic compounds
80 (VOCs) and formation of SOA (Isaacman-VanWertz et al., 2018). Installed with a
81 thermal desorption inlet that collects and heats aerosol to evaporate organic compounds,
82 e.g. Filter Inlet for Gases and AEROSols (FIGAERO, Lopez-Hilfiker et al., 2014) and
83 Micro Orifice Volatilization Impactor (MOVI, Yatavelli et al., 2012), the CIMS
84 instruments are capable of analyzing particle-phase species and gas-particle partitioning
85 in a semi-continuous way (Stark et al., 2017; Stolzenburg et al., 2018).

86 Although FIGAERO-CIMS has gained recent popularity in atmospheric
87 chemistry research, much of the published work was done in chambers or in the
88 laboratory (D'Ambro et al., 2017, 2018; Hammes et al., 2019; Lopez-Hilfiker et al.,
89 2015). As for the applications in field campaigns, most work has been mostly performed
90 in forest or rural areas (Huang et al., 2019; Hunter et al., 2017; Lee et al., 2016, 2018b),
91 measurements in the urban atmosphere by FIGAERO-CIMS is still limited (Le Breton
92 et al., 2018b). Meanwhile, a systematic analysis on mass spectra of FIGAERO-CIMS
93 in the ambient air is imperative, for a more holistic view in investigating emissions and
94 chemistry of oxygenated organic compounds using FIGAERO-CIMS. In this study, we
95 present the measurement results using FIGAERO-I-CIMS during a coordinated
96 campaign in Guangzhou, a megacity in the Pearl River Region of China. We describe
97 the experimental design, instrumentation setup, calibration and data processing for the
98 FIGAERO-I-CIMS in the campaign. This work will provide a detailed interpretation of
99 the mass spectra of oxygenated species in both gas-phase and particle-phase. The bulk
100 chemical properties will also be discussed to provide an overview of organic
101 compounds.

102 **2 Methods**

103 **2.1 Measurement site and supporting data**

104 Measurements were conducted during the coordinated campaign “Particles,
105 Radicals and Intermediates from oxidation of primary Emissions over the Great Bay
106 Area” (PRIDE-GBA) in October and November 2018. The Great Bay Area (GBA)

107 refers to a highly industrialized and urbanized area in southern China, including two
108 Special Administrative Regions of Hong Kong and Macao, and nine cities surrounding
109 the Pearl River estuary. Affected by the subtropical monsoon climate, the weather in
110 the region was characterized by high temperatures and relative humidity (RH) as well
111 as sufficient sunshine (total solar radiation of the Pearl River Delta region in the fall of
112 2016 was ~ 1200 MJ/m², Liu et al., 2018). The city of Guangzhou lies in the north of
113 the GBA and south of the mountains. Therefore, the city is extensively influenced by
114 both anthropogenic and biogenic emissions. The urban site was located at Guangzhou
115 Institute of Geochemistry, Chinese Academy of Sciences (23.14°N, 113.36°E). Online
116 instruments sampled from inlets set up in laboratories on the eighth-floor or ninth-floor
117 (about 25 meters above the ground).

118 In addition to FIGAERO-I-CIMS discussed later, measurement data from a suite
119 of other instruments were also used in this work. A high-resolution time-of-flight
120 aerosol mass spectrometer (HR-ToF-AMS, Aerodyne Research, Inc.) was deployed to
121 provide chemical composition and many other parameters of ambient aerosol including
122 f60, liquid water content (LWC), particulate organic nitrate and elemental ratios (Hu et
123 al., 2016, 2018). The parameter f60 is the ratio of the integrated signal at m/z 60 to the
124 total signal of organic components and is used as a tracer for biomass burning emissions
125 (Cubison et al., 2011). LWC of aerosol was taken as the sum of water contributed by
126 inorganic components predicted by ISORROPIA II model and organic components
127 calculated based on the organic hygroscopicity parameter (Fountoukis and Nenes, 2007;
128 Guo et al., 2015). Based on AMS data, organic nitrate concentrations were determined
129 by 2-3 times lower NO₂⁺/NO⁺ ratios for organic nitrate than inorganic nitrate (Fry et al.,
130 2013). The calculation method of elemental ratios based on AMS data has been
131 described elsewhere (Aiken et al., 2007; Canagaratna et al., 2015). Detailed information
132 about AMS measurements from the PRIDE-GBA campaign is forthcoming in a separate
133 manuscript. An online GC-MS/FID (Wuhan Tianhong Instrument Co., Ltd) and a
134 proton transfer reaction time-of-flight mass spectrometer (PTR-ToF-MS, Ionicon
135 Analytic GmbH) (Yuan et al., 2017) served as the analytical techniques for measuring
136 isoprene and other VOCs (e.g. monoterpenes, aromatics and a few oxygenated VOCs)

137 (Wu et al., 2020), respectively. Trace gases (CO, O₃, NO and NO₂) were measured by
138 commercial gas monitors (Thermo Fisher Scientific Inc.) (Wang et al., 2020d).
139 Photolysis rates were measured by PFS-100 photolysis spectrometer (Focused
140 Photonics Inc.). Temperature and RH were measured by a Vantage Pro2 weather station
141 (Davis Instruments Corp.). Time series and diurnal profiles of meteorological
142 parameters, trace gases, the photolysis rate of NO₂ (j_{NO_2}) along with several important
143 VOCs (isoprene, monoterpenes, toluene and benzene) are shown in Fig. S1. The
144 temperature during the campaign was between 17 and 33°C with an average of 24°C
145 and RH was between 27 and 97% with an average of 70%.

146 **2.2 FIGAERO-I-CIMS**

147 **2.2.1 Experimental setup**

148 Our instrument consists of a Filter Inlet for Gases and AEROSols (FIGAERO)
149 and a time-of-flight chemical ionization mass spectrometer coupled with an iodide
150 ionization source (Bertram et al., 2011; Lee et al., 2014; Lopez-Hilfiker et al., 2014).
151 The FIGAERO is a multi-port inlet assembly following a two-step procedure
152 alternating between gas mode in which online measurements of gases and semi-
153 continuous sampling of particle-phase species are conducted, and particle mode in
154 which particulate composition is investigated via thermal desorption (Lopez-Hilfiker et
155 al., 2014; Thornton et al., 2020). Iodide source is a “soft” ionization technique with
156 little ionization-induced fragmentation and selective detection towards multi-functional
157 organic compounds, providing elemental compositions for thousands of oxygenated
158 compounds in the atmosphere (Hyytinen et al., 2018; Iyer et al., 2016; Lee et al., 2014;
159 Riva et al., 2019).

160 The sample air was drawn into the ion molecule reaction (IMR) chamber where
161 it intersected and reacted with primary ions generated by flowing 2 mL/min 1000 ppm
162 methyl iodide in 2.4 L/min N₂ through an X-ray source. The pressure in the IMR
163 chamber was maintained at 370-390 mbar. Equipped with a long time-of-flight mass
164 analyzer, our instrument was configured to measure singularly charged ions up to 603

165 Th with a mass resolving power of 10000-11000 ($m/\Delta m$ at 50% height) during the
166 campaign (Fig. S2).

167 Ambient air was continuously sampled through two inlets protruding about 1.5
168 meters out of a window on ninth-floor of a building. One was a 3-meter PFA tubing
169 (1/4-inch OD) for gas phase sampling, through which roughly 9 L/min air was drawn,
170 and 2 L/min was directly taken into the instrument for gas measurements without
171 removing particles, resulting in an inlet residence time of 0.24 seconds. The gas
172 sampling line inside the room was covered by heat insulation associated with a heating
173 cable to minimize condensation on the tubing surface. The other inlet for particle phase
174 was a 3.8-meter metal tubing (3/8-inch OD) fitted with a PM_{2.5} cyclone and a Nafion
175 dryer (Perma Pure, model PD-07018T-12MSS) to reduce water content in the sampled
176 air. The particle phase inlet was drawn by a laminar flow at ~8 L/min (Reynolds number
177 of ~1500), 3.8 L/min of which was collected on PTFE membrane filters (Zefluor[®], Pall
178 Inc., USA). The residence time was 1.3 seconds for the particle phase sampling line.
179 Semi-volatility and low-volatility compounds tend to interact with wall surfaces of both
180 inlets and the IMR and thus extend response time (Krechmer et al., 2016). As accurate
181 correction for wall losses remains impossible, no wall loss correction was performed in
182 this study.

183 The FIGAERO worked in a cyclical 1-hour pattern with two modes (Fig. S3):
184 measuring gas for the first 24 minutes while simultaneously collecting particles on the
185 filter; and then analyzing the particle-phase collection for another 36 minutes. In every
186 24-minute gas mode, ambient air was measured for the first 21 minutes, followed by 3-
187 minute gas background by overflowing zero air at 5 L/min through a pinhole just in
188 front of the IMR. The background measurements are inevitably influenced by wall
189 interactions, especially for “sticky” species. Recently, Palm et al. (2019) proposed a
190 new way to determine gas background (“fast background”) by fast switching between
191 ambient air and background, which greatly improves accurate determination of CIMS
192 background. In the remaining 36 minutes, the components of the collected particles
193 were thermally desorbed and introduced into the CIMS with 2 L/min N₂ carrier gas.

194 The N₂ flow was ramped from ambient temperature to 175°C in 12 minutes and held
195 for another 20 minutes. Schematic diagram of working modes and temperature profile
196 of FIGAERO heating in a single cycle is shown in Fig. S4. Particle background was
197 determined every 6th 1-hour running cycles in which ambient air passed over a filter
198 (Parker Balston, model 9922-11-CQ) in front of the FIGAERO filter.

199 **2.2.2 Calibration experiments**

200 Using various techniques, we calibrated dozens of chemical compounds in the
201 laboratory. Table S1 summarizes the calibrated species and corresponding calibration
202 methods. (1) Gas cylinders are commercially available for a few species (e.g. chlorine,
203 hydrogen cyanide). The gaseous standards were diluted down to different
204 concentrations and then introduced to the CIMS. (2) For those VOCs of which standards
205 are liquid or solid, solutions with known concentrations are made and then vaporized
206 using the liquid calibration unit (LCU, Ionicon Analytic GmbH) to provide gaseous
207 standards. (3) Commercial permeation tubes are available for some species (e.g. nitric
208 acid). (4) Some gaseous chemicals were generated in the laboratory. For example,
209 isocyanic acid was generated from thermal decomposition of cyanuric acid in a
210 diffusion cell (Li et al., 2021; Wang et al., 2020d), and dinitrogen pentoxide was
211 generated via the reaction of ozone with excess nitrogen dioxide in a flow reactor
212 (Bertram et al., 2009). (5) Compounds of low vapor pressure were calibrated through
213 the FIGAERO (Lopez-Hilfiker et al., 2014). Briefly, certain amounts of target species
214 dissolved in organic solvents (e.g. isopropanol or acetone) were deposited onto the
215 PTFE filter of the FIGAERO using a syringe, and the droplet was then subjected to a
216 temperature-programmed thermal desorption by N₂ gas. The sensitivity was determined
217 as the integrated signals under thermogram profiles versus the amounts of deposited
218 calibrant.

219 In addition to sensitivity calibration, the effect of humidity on the sensitivity for
220 various species was investigated in the laboratory, some of which are shown in Fig. S5.
221 Low-molecular-weight acids, e.g., formic acid and nitric acid, tend to be more sensitive
222 to the humidity changes than multi-functional compounds. Similar tendency of multi-

223 functional compounds associated with less humidity dependence was also reported in
224 previous work (Lee et al., 2014). Considering water vapor pressure in the IMR, our
225 humidity-dependent curves are generally consistent with those reported in Lee et al.
226 (2014) (see detailed discussions in Section S3 in the Supplement).

227 In the later part of the campaign (after Oct. 22), an isotopically labeled formic
228 acid (DCOOH, Cambridge Isotope Laboratories, Inc.) permeation tube held at constant
229 temperature (65 °C), was mixed with 10 mL/min N₂ and continuously delivered into
230 the entrance of sampling inlet in order to derive a humidity dependence function from
231 the field measurements. DCOOH signals during the campaign exhibited a humidity-
232 dependent curve consistent with formic acid obtained in the laboratory (Fig. S5). We
233 applied humidity correction to the species with the humidity-dependent curves
234 determined in the laboratory (underlined species in Table S1). For other compounds,
235 humidity correction was not applied, as there is no universal pattern of humidity
236 dependence for all detected species and multi-functional compounds that comprise the
237 majority of the species measured by FIGAERO-I-CIMS are usually less influenced by
238 humidity.

239 The measured concentration of DCOOH was steady after humidity correction
240 was applied (Fig. S6g), indicating the stability of our instrument. In addition, we also
241 performed field calibrations throughout the campaign to check the instrument status by
242 spotting a solution mixture of levoglucosan, heptaethylene glycol and octaethylene
243 glycol onto the FIGAERO filter every 2-3 days (Fig. S6). Multiple-point calibrations
244 for these organic species were performed in the beginning and the end of the campaign.
245 The concentration of the solution used in the first two calibration experiments was too
246 high, so we prepared a new solution for calibrations in November. The relative changes
247 of the determined calibration factors in November were within 50% for the calibrated
248 species.

249 **2.2.3 Data processing**

250 The TofWare software (version 3.0.3; Tofwerk AG, Switzerland) was used to
251 conduct the high-resolution peak fitting for the mass spectra data of ToF-CIMS,

252 including mass calibration, instrumental parameters optimization (peak shape and peak
253 width) and bunch fitting of high-resolution peaks (Stark et al., 2015). In this study, the
254 signals of ions were normalized to the sum signals of I^- and H_2OI^- at 10^6 cps.
255 Hourly particle-phase data were obtained by integrating the signals of various ions
256 during each FIGAERO desorption period. Background corrected signals were obtained
257 by subtracting linearly interpolated background signals from ambient signals (and
258 integrated signals) for ions in the gas (and particle) phase.

259 In order to determine the sensitivities of uncalibrated species, voltage scanning
260 procedure was performed from time to time throughout the campaign covering different
261 times of the day (Iyer et al., 2016; Lopez-Hilfiker et al., 2016). Here, we selected four
262 representative periods including morning, afternoon, evening and night on polluted
263 days. By performing sigmoidal fitting on the remaining signals as a function of voltages,
264 a dV_{50} value of each ion from each period was determined at which voltage half of one
265 kind of ion dissociated (Lopez-Hilfiker et al., 2016). We observed a positive correlation
266 between the sensitivities of the ions relative to maximum sensitivity and their average
267 dV_{50} values (Fig. S7), consistent with previous studies (Isaacman-VanWertz et al., 2018;
268 Lopez-Hilfiker et al., 2016). This relationship was used to calculate response factors for
269 uncalibrated species, after taking into account the relative transmission efficiency for
270 the ions (see Section S1 in the Supplement for detailed analysis).

271 **3 Results and discussion**

272 **3.1 Overview of detected species in the mass spectra**

273 We identify 1334 ions adducted with iodide from the mass spectra, among which
274 427 are charged closed-shell organic compounds containing only C, H, O elements
275 ($C_xH_yO_zI^-$) and 388 are charged closed-shell organic compounds containing C, H, O
276 and N elements ($C_xH_yN_{1,2}O_zI^-$). For species with the formula of $C_xH_yO_z$, x ranges
277 from 1 to 20; y is an even number and no more than $2x+2$; z is greater than or equal to
278 2. The range of carbon number x for the ions with $C_xH_yN_{1,2}O_z$ is the same as the ions
279 with $C_xH_yO_z$. For species containing one nitrogen ($C_xH_yNO_z$), y is an odd number and
280 less than $2x+2$; z is larger than or equal to 2. For species containing two nitrogen atoms

281 ($C_xH_yN_zO_z$), y is an even number and less than $2x+1$; z is larger than or equal to 4.
282 Table 1 summarizes species discussed in the main text. Although iodide clusters with
283 two nitrogen atoms and zero nitrogen atoms both lie on odd masses, they can be
284 separated for certain ions with the current resolving power, as demonstrated by the peak
285 fitting results of mass spectrum at m/z 311 (Fig. S8).

286 The campaign-averaged mass spectra of detected ions in the both gas and particle
287 phases are shown in Fig. 1. In general, molecules in particle-phase have larger
288 molecular weights compared to those in gas-phase. Signals in the mass range of 150-
289 300 Th comprise a large fraction of gas-phase compounds, and concentrations in the
290 gas phase decrease quickly with m/z higher than 250 Th. In contrast, the detected
291 signals in the particle phase are mainly distributed within the range of 200-320 Th.

292 Average nighttime (10 pm - 6 am) and daytime (10 am - 6 pm) mixing ratios for
293 various species were shown in Fig. 2. Most species have higher concentrations during
294 the daytime, especially for relatively volatile compounds in gas-phase, despite the fact
295 that lower boundary layer height at night should increase nighttime concentration, as
296 many primary gases behaved, e.g. CO (Fig. S1) (Wu et al., 2020). The higher
297 concentrations during the daytime for most species detected by FIGAERO-I-CIMS
298 suggest the dominant role of photochemical induced oxidation in forming these
299 oxidized compounds. In addition to typical nocturnal species including nitryl chloride
300 ($ClNO_2I^-$), chlorine nitrate ($ClONO_2I^-$) and dinitrogen pentoxide ($N_2O_5I^-$), higher
301 concentrations for the ions of $C_6H_{10}O_5I^-$ and $C_6H_{12}O_5I^-$ were also observed, which
302 will be discussed in the next section. A large number of particulate N-containing organic
303 compounds increase at night as well, as shown by mass defect diagrams of $C_xH_yO_z$
304 and $C_xH_yN_{1,2}O_z$ color coded by the night to day ratios (Fig. S9).

305 Based on the mass spectra shown in Fig. 1, we identify a number of ions
306 associated with high concentrations in both gas and particle phases. In the following
307 Section 3.2-3.7, we will perform interpretation of the mass spectra by analyzing
308 variability and correlation of these important ions, including monosaccharide-derived
309 compounds (with brown tags in Fig. 1), oxygenated aromatics (with purple tags),
310 organic acids (with pink tags), oxidation products of biogenic volatile organic

311 compounds (BVOCs, with green tags), sulfur-containing compounds, and inorganics
312 (with blue tags). After going through detailed analysis at the species level, Section 3.8
313 will provide an overall picture about bulk chemical characteristics of detected organic
314 compounds in terms of the distributions of average carbon oxidation states, carbon
315 number and oxygen number. Lastly, Section 3.9 will compare our measurement of
316 organic aerosol (OA) with AMS data.

317 **3.2 Monosaccharide-derived compounds**

318 $C_6H_{10}O_5$ and $C_6H_{12}O_5$ are highly correlated with each other in aerosol ($r=0.92$),
319 and they are two of the few $C_xH_yO_z$ compounds with higher concentrations at night.
320 Previous work assigned them as monosaccharide derived compounds emitted from
321 biomass burning (Bhattacharai et al., 2019; Qi et al., 2019; Reyes-Villegas et al., 2018;
322 Simoneit et al., 1999).

323 In this campaign, $C_6H_{10}O_5$ was detected mostly in the particle phase (the fraction
324 in the particle phase $F_p=0.81\pm 0.09$) with an average concentration of 0.073 ± 0.076
325 $\mu\text{g}/\text{m}^3$. Its diurnal profile started increasing at dusk, reaching a peak at about midnight
326 and then fell off, as shown in Fig. 3. The mass fraction of $C_6H_{10}O_5$ in OA had a similar
327 diurnal profile, and the ratios of $C_6H_{10}O_5$ to CO increased at night (from 0.17 ± 0.02 to
328 $0.5\pm 0.03 \mu\text{g}\cdot\text{m}^{-3}/\text{ppm}$, Fig. 3c), both suggesting enhanced emissions of this compound
329 were related with combustion activities in the evening, e.g., residential biofuel burning
330 for cooking as reported by some previous measurements in China (Wang et al., 2020c;
331 Zhang et al., 2015). Furthermore, the time variations of particle-phase $C_6H_{10}O_5I^-$
332 were very similar to those of the m/z 60 fragment in AMS mass spectra (Fig. 3a), which
333 is an identified tracer of biomass burning OA produced from the thermal decomposition
334 of levoglucosan and similar compounds on the vaporizer of AMS (Brege et al., 2018;
335 Cubison et al., 2011; Schneider et al., 2006). Therefore, $C_6H_{10}O_5$ was probably
336 levoglucosan and its isomers (mannosan and galactosan), and $C_6H_{12}O_5$ was probably
337 also a monosaccharide compound that had similar sources to $C_6H_{10}O_5$.

338 **3.3 Oxygenated aromatic compounds**

339 Combustion activities emit a great deal of compounds besides saccharides that
340 the I-CIMS instrument can detect including nitro-aromatics and guaiacol derivatives
341 (Gaston et al., 2016; Kong et al., 2021). Nitro-benzenediols ($C_6H_5NO_4I^-$) as well as
342 the highly correlated homologue methyl nitro-benzenediols ($C_7H_7NO_4I^-$) ($r=0.88$ in
343 the particle phase), exhibited double peaks in their diurnal profiles (Fig. 4). One was in
344 the evening, similar to levoglucosan ($C_6H_{10}O_5$). The other peak was at noon. The
345 scatterplot of $C_6H_5NO_4$ as the function of $C_6H_{10}O_5$ exhibits two different slopes (Fig.
346 5): the lower slope at night (0.088 ± 0.005) indicates the contribution of biomass burning,
347 while the higher slope during the daytime (0.26 ± 0.02) suggests there were other
348 important sources for nitro-aromatics, potentially secondary formation from
349 photooxidation of aromatics (Jenkin et al., 2003). Guaiacol derivatives may have
350 similar sources with nitro-aromatics, as implied by the resemblance of the scatterplots
351 of these two chemical classes versus levoglucosan (cf., Fig. S10 and Fig. 5).

352 Nitrophenols ($C_6H_5NO_3I^-$), methyl nitrophenols ($C_7H_7NO_3I^-$) and
353 dinitrophenols ($C_6H_4N_2O_5I^-$) were the most significant components of nitro-aromatics
354 in the gas phase. Despite the fact that nitrated phenols could be formed by
355 photochemical oxidation of their aromatic hydrocarbon precursors (Wang et al., 2020a;
356 Yuan et al., 2016), none of them peaked in the daytime, consistent with a previous
357 proposal on photolysis as the dominant loss pathway for these compounds (Chen et al.,
358 2011; Yuan et al., 2016). $C_6H_5NO_3$ and $C_7H_7NO_3$ peaked in the evening, suggesting
359 important contributions of NO_3 -induced reactions and/or primary emissions. The peak
360 time of $C_6H_4N_2O_5$ was later than that of $C_6H_5NO_3$, in agreement with dinitrophenols as
361 the oxidation products from nitrophenols (Harrison et al., 2005).

362 We also detected non-N-containing compounds that were identified as oxidation
363 products of aromatics in the literature, including $C_7H_6O_4I^-$, $C_7H_8O_4I^-$ and
364 $C_7H_8O_5I^-$ (Mehra et al., 2020; Schwantes et al., 2017). $C_7H_6O_4$ and $C_7H_8O_4$ correlated
365 well with each other ($r=0.72$ in gas-phase and 0.91 in particle-phase). High
366 concentrations of $C_7H_6O_4$ and $C_7H_8O_4$ were mainly observed during the periods with
367 lower NO_x concentration, which was a contrast to the variations of nitrophenols (Fig.
368 S10). In addition, the concentration ratios of $C_7H_8O_4I^-$ and $C_7H_7NO_3I^-$ are lower

369 for higher NO_x concentration (Fig. 5), consistent with the literature that the formation
370 of C₇H₆O₄ and C₇H₈O₄ is suppressed at high NO_x concentration (Schwantes et al.,
371 2017). C₇H₈O₅ is reported as the ring-retaining oxidation product of C₇H₈O₄ which is a
372 typical oxidation product of toluene and cresol (Schwantes et al., 2017; Wang et al.,
373 2020b), as well as the ring-scission products of aromatic hydrocarbons with more
374 carbon atoms, e.g. trimethyl benzenes (Mehra et al., 2020). Given that C₇H₈O₅ closely
375 followed with C₇H₈O₄ ($r=0.93$ in particles), toluene oxidation was probably the main
376 contributor to this compound.

377 **3.4 Organic acids and related compounds**

378 Organic acids were one of the most abundant species classes detected by I-CIMS
379 (Fig. 1). Low-molecular-weight organic acids (e.g., formic, acetic, glycolic and pyruvic
380 acid) constituted a significant fraction of signals in the mass spectra of the gas phase.
381 As shown in Fig. 6 (and also Fig. S11), they had very similar temporal trends with
382 diurnal maxima in the afternoon, indicating photochemical oxidation played a dominant
383 role in their formation (de Gouw et al., 2018; Yuan et al., 2015).

384 In contrast to monocarboxylic acids, dicarboxylic acids partitioned mostly to
385 particle-phase. As the dominant dicarboxylic acids in aerosol (Kawamura and Bikkina,
386 2016; Mellouki et al., 2015), $94\pm 5\%$ and $74\pm 13\%$ (mean \pm one standard deviation of
387 F_p) of C₂H₂O₄ and C₃H₄O₄, assigned as oxalic and malonic acid, were found in particle-
388 phase, respectively. The concentrations of C₄H₆O₄ were significantly lower compared
389 to C₂ and C₃ homologous series, but C₅H₈O₄ and C₆H₁₀O₄ had unexpected high
390 abundance (Fig. 7). Additionally, C₅H₈O₄ and C₆H₁₀O₄ had considerable fractions in
391 the gas phase ($45\pm 13\%$ and $43\pm 11\%$), significantly higher than their C₂-C₃
392 homologous series. These two compounds were correlated well with each other in
393 temporal variations ($r=0.97$ and 0.91 in the gas and particle phases, respectively), and
394 their diurnal variations were different from those of oxalic and malonic acid (Fig. 6).
395 Therefore, dicarboxylic acids may not be the dominant contributing species for the two
396 compounds. C₅H₈O₄ and C₆H₁₀O₄ have been observed from previous studies on
397 isoprene oxidation (Berndt et al., 2018, 2019), attributing them as epoxy hydroperoxyl

398 carbonyl and accretion product, respectively. However, the relative contributions from
399 these possibilities remain unclear.

400 In addition to the series of $C_nH_{2n-2}O_4$ (i.e. $C_2H_2O_4$, $C_3H_4O_4$), we also observed
401 comparable concentrations of $C_nH_{2n-4}O_4$ series, especially for carbon number of 4
402 and 5 ($C_4H_4O_4$ and $C_5H_6O_4$). Considering the double bonds in the molecules,
403 $C_nH_{2n-4}O_4$ should be more reactive than $C_nH_{2n-2}O_4$, suggesting there were large
404 sources for these compounds. Previous studies have reported photo-oxidation of
405 aromatics can generate $C_nH_{2n-4}O_4$, including $C_4H_4O_4$ and $C_5H_6O_4$ (Brege et al., 2018;
406 Kawamura et al., 1996; Kawamura and Bikkina, 2016). Our measurements showed that
407 temporal trends of $C_4H_4O_4$ and $C_5H_6O_4$ followed well with those of aromatic
408 hydrocarbons (Fig. S11b), and thus oxidation of aromatics could be an important
409 contributor to $C_nH_{2n-4}O_4$ in the urban air.

410 **3.5 Oxidation products of Biogenic VOCs**

411 In addition to high anthropogenic emissions of aromatics, terrestrial vegetations
412 nearby also released significant amounts of biogenic VOCs (BVOCs) (Wu et al., 2020).
413 During the campaign, the concentrations of isoprene at noon were between 0.1 and 1.5
414 ppb, whereas the range of daily maxima of monoterpenes was 0.05-2.5 ppb. Hence, a
415 number of oxidation products of BVOCs were detected (Fig. 8 and Fig. S12).

416 The ion $C_4H_7NO_5I^-$ was the most abundant N-containing C4 organic
417 compounds that were detected in the gas phase. Its daily maxima occurred in the
418 afternoon and correlated moderately with methyl vinyl ketone (MVK) + methacrolein
419 (MACR) measured by PTR-ToF-MS (Fig. 8b, $r=0.58$). We consequently assigned
420 $C_4H_7NO_5$ as MVK nitrates and MACR nitrates, which were reported as the second
421 generation of organic nitrates formed from the oxidation of isoprene hydroxynitrates by
422 OH in the presence of NO_x (Fisher et al., 2016; Paulot et al., 2009). Strong correlations
423 were observed between $C_5H_9NO_4I^-$, $C_5H_9NO_5I^-$ and $C_4H_7NO_5I^-$ ($r=0.93$ and 0.80 ,
424 respectively), which was in accordance with their similar formation pathways (Jacobs
425 et al., 2014; Wennberg et al., 2018; Xiong et al., 2015). Hence, we expected these three
426 compounds were common oxidation products of isoprene in the polluted atmosphere.

427 While in aerosol, 2-methylglyceric acid ($C_4H_8O_4$) is a commonly reported oxidation
428 product of isoprene formed in high- NO_x conditions (Surratt et al., 2010). We observed
429 the corresponding ion $C_4H_8O_4I^-$ contributing to OA especially in dry conditions with
430 strong sunlight (Fig. S13). This evidence indicates that isoprene oxidation may
431 contribute to $C_4H_8O_4$, but potential contribution from other sources cannot be ruled out
432 in urban areas.

433 In terms of monoterpenes, a reasonable correlation (Fig. S14a, $r=0.63$) was found
434 between the ions $C_{10}H_{16}O_3I^-$ and $C_{10}H_{16}O_2H^+$ measured by PTR-ToF-MS.
435 $C_{10}H_{16}O_2H^+$ was attributed to pinonaldehyde formed from the oxidation of
436 monoterpenes (Glasius et al., 2000; Larsen et al., 2001; Mutzel et al., 2016). Therefore,
437 we tentatively assign $C_{10}H_{16}O_3I^-$ as pinonic acid and its oxocarboxylic acid isomers,
438 which are formed via the oxidation of pinonaldehyde (Fang et al., 2017). $C_8H_{13}NO_6$
439 also exhibited enhanced gas-phase formation during the day as pinonic acid did. The
440 correlation coefficient of the two compounds was 0.71. In contrast to other monoterpene
441 nitrates, particle-phase $C_8H_{11}NO_7$ and $C_{10}H_{15}NO_6$ peaked at night and decreased during
442 the daytime (Fig. S12), indicative of the role of NO_3 in producing organic nitrates as
443 reported in the literature (Faxon et al., 2018). However, $C_{10}H_{15}NO_6$ in the gas phase
444 showed a distinct diurnal profile with peak before the noon. Two possible types of
445 compounds were proposed for $C_{10}H_{15}NO_6$ in previous studies: peroxyacetyl nitrate
446 from pinonaldehyde (Faxon et al., 2018; Nah et al., 2016; Schwantes et al., 2020), or
447 organic nitrates (Bean and Hildebrandt Ruiz, 2016; Boyd et al., 2015). Given the
448 distinct diurnal profiles of $C_{10}H_{15}NO_6I^-$ in the gas and particle phases and the fact
449 that peroxyacetyl nitrate is supposed to dissociate during the FIGAERO heating
450 (Slusher et al., 2004), we speculate that both compounds contributed to this ion. As
451 shown in Fig. S15, $C_8H_{12}O_4$ and $C_9H_{14}O_4$ existed mostly in particle-phase
452 ($F_p=0.63\pm 0.11$ and 0.67 ± 0.10 , respectively). We interpret them as products of
453 monoterpenes via photochemical processes, consistent with the interpretations
454 presented in previous work (Mohr et al., 2013; Mutzel et al., 2015).

455 **3.6 S-containing compounds**

456 Organosulfates are concerned as important components of SOA (Hallquist et al.,
457 2009; Surratt et al., 2007), and they can be detected by iodide anion via proton
458 abstraction (Le Breton et al., 2018b; Lee et al., 2014). We detected the ion $C_2H_3SO_6^-$
459 with a diurnal peak in the afternoon (Fig. 9). This ion was attributed to glycolic acid
460 sulfate, as suggested by previous work (Galloway et al., 2009; Liao et al., 2015).

461 Abundant SO_3I^- was detected in particles, and it correlated well with the ion
462 $C_2H_3SO_6^-$ (Fig. 9b) and sulfates measured by AMS (Fig. S16). Previous work observed
463 the sulfite ion radical ($\cdot SO_3^-$) during the ionization of organosulfates in a liquid
464 chromatography-electrospray ionization-tandem mass spectrometer (Huang et al.,
465 2018). As a result, the ion SO_3I^- from FIGAERO-I-CIMS might be a potential
466 indicator for the total organosulfates. However, more future work is needed for
467 evaluating this possibility.

468 Other sulfate-related ions during gas-phase modes were also detected including
469 HSO_4^- (sulfuric acid), $CH_3SO_3^-$ (methanesulfonic acid) which were enhanced in the
470 gas phase during the daytime, in agreement with the notions of photochemistry-induced
471 gas-phase oxidation (Brandt and van Eldik, 1995). However, these data were not
472 available for quantification given that these low-volatile species would condense on our
473 long gas sampling inlet. It should be noted that measuring sulfuric acid in the gas-phase
474 is difficult and generally requires a “wall-less” source design (Eisele and Tanner, 1993).

475 **3.7 Inorganic compounds**

476 There is a growing interest in N_2O_5 and its product nitryl chloride ($ClNO_2$)
477 because $ClNO_2$ is found to serve as a nocturnal reservoir of Cl radical and reactive
478 nitrogen, and hence enhance the ozone formation the next day (Osthoff et al., 2008;
479 Wang et al., 2016). Time series of N_2O_5 and $ClNO_2$ exhibited two patterns. During most
480 of the nights, N_2O_5 started to increase quickly at sunset and lasted for only 2-3 hours,
481 and $ClNO_2$ increased in the meantime and ultimately reached its maximum at night,
482 indicative of local formation of $ClNO_2$. However, sometimes a high level of N_2O_5 did
483 not lead to an increase in $ClNO_2$ (tinted background in Fig. 10a), probably due to the
484 lack of chloride salts on the aerosol. Other nocturnal species including $ClONO_2$ and Cl_2

485 were highly correlated with ClNO_2 as expected ($r=0.92$ and 0.83 , respectively),
486 suggesting they had common formation mechanisms (Liu et al., 2017).

487 HNO_3I^- was observed as one of the most abundant species in the mass spectra
488 of FIGAERO-I-CIMS both in the gas and particle phases. In the gas phase, the ion
489 HNO_3I^- from I-CIMS has been used to quantify nitric acid (Lee et al., 2018a). The
490 concentrations of gas-phase nitric acid peaked in the afternoon, suggesting
491 photochemistry in the daytime as the dominant source for gas-phase nitric acid.

492 Previous study suggested that HNO_3I^- from particle-phase measurement by
493 FIGAERO-I-CIMS can be indicative of nitrate in the particle phase (Lee et al., 2016).
494 Here, the concentrations of HNO_3I^- in the particle phase were compared with
495 particulate nitrate measured by AMS (Fig. 11c). Strong correlation was observed
496 ($r=0.93$), but the concentrations measured by FIGAERO-I-CIMS were higher
497 (slope=1.6), especially for higher concentrations of organic nitrates. Using a threshold
498 of $1 \mu\text{g}/\text{m}^3$ for organic nitrates, the slopes and correlations were higher for the data
499 points with particulate organic nitrates larger than $1 \mu\text{g}/\text{m}^3$ (slope=1.8, $r=0.94$) than
500 those less than $1 \mu\text{g}/\text{m}^3$ (slope=1.1, $r=0.90$). In short, our measurements suggest that
501 HNO_3I^- in the particle phase from FIGAERO-I-CIMS are formed from thermal-
502 decomposition of both inorganic nitrate (e.g. NH_4NO_3) and organic nitrates.

503 **3.8 Bulk chemical properties of detected organic compounds**

504 The above discussions on individual chemical groups provide insights into the
505 identification of the mass spectra from FIGAERO-I-CIMS, along with sources and
506 chemistry of oxygenated organic compounds in the urban atmosphere. In this section
507 and the following one, we will provide a bulk analysis of the detected organic
508 compounds.

509 Organic compounds detected by FIGAERO-I-CIMS were comprehensively
510 characterized with detailed elementary composition in $\overline{\text{OS}}_C - n_C$ space (Fig. 12)
511 which depicts the average oxidation states of carbon for closed-shell $\text{C}_x\text{H}_y\text{O}_z$ and
512 $\text{C}_x\text{H}_y\text{N}_{1,2}\text{O}_z$ compounds as a function of carbon number. The details in calculation of
513 $\overline{\text{OS}}_C$ can be found in Section S2 in SI. S-containing compounds were omitted given

514 their negligible variety and concentration compared to $C_xH_yO_z$ and $C_xH_yN_{1,2}O_z$. The
515 average \overline{OS}_C in the particle phase was higher than that in the gas phase at the same
516 carbon number, especially for carbon number between 2 and 10. This agrees with our
517 expectation that more oxidized compounds would partition more strongly in aerosol, as
518 indicated by larger fractions in particles (Fp) for higher \overline{OS}_C . In addition, the average
519 \overline{OS}_C generally increased for lower carbon number, as a result of functionalization and
520 fragmentation during VOCs aging. However, there was a notable exception in C5 which
521 had a significantly reduced \overline{OS}_C , probably as the result of emissions of isoprene. The
522 analysis of the $\overline{OS}_C - n_C$ space indicates that the large number of organic compounds
523 measured by FIGAERO-I-CIMS are useful to characterize the evolution of organic
524 compounds in the atmosphere.

525 The distributions of carbon and oxygen numbers of organic compounds were also
526 investigated, as shown in Fig. 13. Most abundant organic compounds measured by
527 FIGAERO-I-CIMS were C2-C3 compounds, which accounted for about 66% in the gas
528 phase and 56% in the particle phase. It is unexpected that C2-C3 compounds made up
529 such a significant portion in the particle phase, indicating a non-negligible role of
530 thermal decomposition from low volatility compounds such as accretion products or
531 extremely low volatile organic compounds which were reported from FIGAERO
532 measurements on SOA (D'Ambro et al., 2018; Lopez-Hilfiker et al., 2014; Stark et al.,
533 2017). Organic compounds with carbon numbers over 5 constituted only 3% in the gas
534 phase, while they accounted for 30% in the particle phase. The oxygen numbers of the
535 majority of gaseous organic compounds were no more than 3. Organic compounds
536 containing 2-3 oxygen atoms had the largest contribution in both gas-phase (96%) and
537 particle-phase (56%). $C_xH_yN_{1,2}O_z$ accounted for less than 10% of the total oxygenated
538 organic compounds. In the gas phase, compounds with 5-6 oxygen atoms accounted for
539 51% of $C_xH_yN_{1,2}O_z$, indicative of the high levels of organic nitrates in the urban
540 atmosphere. Nitrophenols also contributed significantly to $C_xH_yN_{1,2}O_z$ compounds,
541 as they accounted for 74% of $C_xH_yN_{1,2}O_z$ containing 3 oxygen atoms, which in turn
542 contributed to 22% of $C_xH_yN_{1,2}O_z$. In contrast, in the particle phase, the oxygen

543 numbers of $C_xH_yN_{1,2}O_z$ distributed relatively evenly, as the fractions of compounds
544 with 3-8 oxygen atoms were similar (between 12% and 19%). Compared to
545 measurements in a forest in the southeastern United States (cf., Table S1 from Lee et
546 al., 2016), the fractions of N-containing organic compounds with less than 5 oxygen
547 atoms were significantly larger in our measurements as a result of higher concentrations
548 of nitro-aromatics.

549 We further determined the fractions of N-containing organic compounds in total
550 organic compounds as a function of m/z. It is clear that the observed fractions of N-
551 containing organic compounds were higher for elevated m/z (Fig. 14) and N-containing
552 ions commonly dominated at even nominal masses (Fig. S17). The gas-phase CHON
553 ions within the m/z range of 250-350 Th accounted for about half of the organic
554 compounds in this range. The fractions of CHON ions in particle-phase were somewhat
555 smaller than those in the gas phase within the above m/z range, but were comparable
556 for higher m/z. A possible explanation for this is that functional groups of nitrate and
557 nitro reduce less in vapor pressure for organic compounds than functional groups of
558 carboxylic or oxygen-equivalent hydroxyl do (Capouet and Müller, 2006; Nannoolal et
559 al., 2008; Pankow and Asher, 2008). Consequently, CHON compounds are generally
560 more volatile than CHO compounds with similar molecular weights.

561 In the end, we determined the total concentration of N-containing organic
562 compounds in the particle phase measured by FIGAERO-I-CIMS and compared it with
563 the particulate organic nitrates derived from AMS (Fig. 15). Good agreement was
564 achieved when the concentration of inorganic nitrate was relatively low, e.g. below 8
565 $\mu\text{g}/\text{m}^3$. However, the discrepancies increased when inorganic nitrate concentration
566 increased, which can affect the determination of organic nitrate from AMS. This
567 encouraging result indicates that FIGAERO-I-CIMS is able to capture the variability of
568 organic nitrates in the urban atmosphere, which can be helpful in understanding the
569 sources and formation mechanism of these compounds.

570 **3.9 Organic aerosol measurements**

571 The total concentration of organic compounds in the particle phase measured by
572 FIGAERO-I-CIMS was determined and compared with measurements of OA by AMS.
573 The total organic compounds measured by FIGAERO-I-CIMS explained $24 \pm 0.8\%$
574 (fitted slope \pm one standard deviation) of the total OA in average (Fig. 16a), which is
575 lower than the average fractions ($\sim 50\%$) reported previously in boreal and temperate
576 forests (Lopez-Hilfiker et al., 2016; Stark et al., 2017). The lower fractions determined
577 here might be the result of larger contributions to OA from primary emissions in the
578 urban air, which are composed of a large number of compounds with little signals in I-
579 CIMS (Zhao et al., 2016). As shown in Fig. 16a, organic compounds measured by
580 FIGAERO-I-CIMS accounted for higher fractions in OA concentrations by AMS for
581 more aged OA, consistent with the fact that I-CIMS are more sensitive to oxygenated
582 organic compounds with multiple functional groups (Lee et al., 2014; Lopez-Hilfiker
583 et al., 2016). Furthermore, we expect this fraction to change with the relative
584 contributions of primary emissions and secondary formation for organic compounds in
585 the atmosphere. Similar trends were found in Le Breton et al. (2019), in which an
586 acetate source was used. Acetate ions have been reported to selectively ionize highly
587 oxygenated organic compounds as an iodide source does (Aljawhary et al., 2013).

588 Comparison of the Van Krevelen diagrams between FIGAERO-I-CIMS and
589 AMS also provides useful insights on the measurement of organic compounds in OA.
590 The Van Krevelen diagram has been used as a tool for analyzing functional groups and
591 OA aging by plotting H/C ratios versus O/C ratios (Heald et al., 2010; Lambe et al.,
592 2012). As shown in Fig. 16b, the data points of the bulk OA from FIGAERO-I-CIMS
593 followed the same trend as the data points from AMS. However, the bulk OA measured
594 by FIGAERO-I-CIMS only occupied a much smaller region with O/C ratios between
595 0.7 and 1.0. We further plotted all of the organic compounds in the H/C versus O/C
596 space color-coded with their campaign-average concentrations (Fig. S18a). We
597 observed that most data points from FIGAERO-I-CIMS distributed across the zone
598 between the slope of 0 and -1.0. These observations provide additional evidence that
599 FIGAERO-I-CIMS may only measure the more oxidized organic compounds in OA.

600 The correlation coefficients between the particle phase concentrations at unit
601 masses by FIGAERO-I-CIMS and OA mass concentration by AMS were calculated
602 (Fig. S18b). The correlation coefficients were small for ions below m/z 200, as these
603 ions contributed little to organic aerosol. Moderate and strong correlations ($r > 0.7$) were
604 observed for the ions of m/z between 200 and 400 Th, implying that organic compounds
605 with molecular weights of 100-300 g/mol may account for significant fractions in
606 organic aerosol. The possible reason for the lower correlations for heavier compounds
607 ($m/z > 400$ Th) with OA mass loadings is that these compounds might be related to
608 specific sources or certain chemical processes, which might not contribute at large
609 fractions to the total OA concentration.

610 **4 Summary**

611 We deployed a FIGAERO-I-CIMS instrument to measure oxygenated organic
612 compounds in both gas phase and particle phase at a representative urban site in China.
613 The experimental design and instrumentation setup were described in detail, which goes
614 above and beyond typical studies, including (1) performing sensitivity calibrations in
615 the laboratory using multiple methods for multiple species; (2) performing voltage
616 scanning for unknown compounds detected in the ambient air; (3) performing humidity
617 calibrations for multiple types of species, which we have not seen anyone do after Lee
618 et al. (2014).

619 From the mass spectra, a number of important compounds in the urban
620 atmosphere were identified. We detected high concentrations of several
621 monosaccharide species (e.g., levoglucosan). They were potentially emitted from
622 biomass burning which also contributed to the enhancement of many nitro-aromatic
623 species. Photochemistry was also found to be a strong source of nitro-aromatics. Low-
624 molecular-weight organic acids were mainly observed in the gas phase, and
625 observations supported daytime photochemistry as the dominant source. Different
626 diurnal profiles for various BVOC-derived organic nitrates were observed, reflecting
627 their different formation pathways related to NO_x chemistry (i.e. daytime photo-
628 oxidation, nocturnal NO_3 reactions). Local formation of nitryl chloride was observed,

629 highlighting the potential importance of nighttime chemistry in the urban region. Our
630 measurements show that oxygenated organic compounds dominated the majority of
631 detected species by FIGAERO-I-CIMS, in which CHO and CHON compounds both
632 accounted for significant fractions. Nitrogen-containing organic compounds occupied
633 a significant fraction of the total signals in both the gas and particle phases, with
634 elevated fractions at higher molecular weights. The most abundant organic compounds
635 were formic acid and multifunctional organic compounds containing 3-5 oxygen atoms.
636 Organic compounds containing 2-3 carbon atoms accounted for over half of the total
637 organic compounds in both gas- and particle-phase measured by FIGAERO-I-CIMS.
638 During the campaign, the FIGAERO-I-CIMS measurements explained $24\pm 0.8\%$ of OA
639 mass measured by AMS, but the fractions were higher for more aged organic aerosol.
640 This evidence, along with the analysis of the Van Krevelen plot, indicates that
641 FIGAERO-I-CIMS is measuring the more oxidized fraction of OA in the urban air.

642 Our observations suggest that oxygenated organic compounds in urban
643 environments are complicated in both sources and chemistry. Oxygenated organic
644 compounds can be both emitted from various emission sources (e.g. vehicular
645 emissions and biomass burning) and also secondary produced in the atmosphere. The
646 chemistry in forming and removing these oxygenated organic compounds can be
647 associated with daytime and nocturnal reactions initiated from both anthropogenic and
648 biogenic precursors with strong influences from NO_x chemistry. This work
649 demonstrates that the rich information in both gas and particle phases provided by
650 FIGAERO-I-CIMS can greatly promote the understanding of emission and chemistry
651 of organic carbon in the atmosphere of urban regions.

652

653 **Acknowledgement**

654 This work was supported by the National Key R&D Plan of China (grant No.
655 2019YFE0106300, 2018YFC0213904, 2016YFC0202206), the National Natural
656 Science Foundation of China (grant No. 41877302), Guangdong Natural Science
657 Funds for Distinguished Young Scholar (grant No. 2018B030306037), Guangdong

658 Provincial Key R&D Plan (grant No. 2019B110206001), Guangdong Soft Science
659 Research Program (grant No. 2019B101001005) and Guangdong Innovative and
660 Entrepreneurial Research Team Program (grant No. 2016ZT06N263). This work was
661 also supported by Special Fund Project for Science and Technology Innovation Strategy
662 of Guangdong Province (Grant No.2019B121205004). Weiwei Hu and Wei Chen were
663 supported by National Natural Science Foundation of China (41875156).

664 **Data availability**

665 The more detailed data can be provided by contacting the corresponding authors.

666 **Author contributions**

667 BY and MS designed the research. CSY, YL, ZLW, TGL, WWH, WC, CHW,
668 CMW, SH, JPQ, BLW, CW, WS, XMW, ZYZ, XMW contributed to data collection.
669 CSY performed the data analysis with contributions from WWH and WC. CSY and
670 BY prepared the manuscript with contributions from JEK and other authors. All the
671 authors reviewed the manuscript.

672 **Competing interest**

673 The authors declare that they have no conflicts of interest.

674

675

676 **References**

677 Aiken, A. C., DeCarlo, P. F. and Jimenez, J. L.: Elemental Analysis of Organic
678 Species with Electron Ionization High-Resolution Mass Spectrometry, *Anal. Chem.*,
679 79(21), 8350–8358, doi:10.1021/ac071150w, 2007.
680 Aljawhary, D., Lee, A. K. Y. and Abbatt, J. P. D.: High-resolution chemical
681 ionization mass spectrometry (ToF-CIMS): Application to study SOA composition
682 and processing, *Atmos. Meas. Tech.*, 6(11), 3211–3224, doi:10.5194/amt-6-3211-
683 2013, 2013.

684 Bean, J. K. and Hildebrandt Ruiz, L.: Gas-particle partitioning and hydrolysis of
685 organic nitrates formed from the oxidation of alpha-pinene in environmental chamber
686 experiments, *Atmos. Chem. Phys.*, 16(4), 2175–2184, doi:10.5194/acp-16-2175-2016,
687 2016.

688 Berndt, T., Scholz, W., Mentler, B., Fischer, L., Herrmann, H., Kulmala, M. and
689 Hansel, A.: Accretion Product Formation from Self- and Cross-Reactions of RO₂
690 Radicals in the Atmosphere, *Angew. Chemie Int. Ed.*, 57(14), 3820–3824,
691 doi:10.1002/anie.201710989, 2018.

692 Berndt, T., Hyttinen, N., Herrmann, H. and Hansel, A.: First oxidation products from
693 the reaction of hydroxyl radicals with isoprene for pristine environmental conditions,
694 *Commun. Chem.*, 2(1), 1–10, doi:10.1038/s42004-019-0120-9, 2019.

695 Bertram, T. H., Thornton, J. A. and Riedel, T. P.: An experimental technique for the
696 direct measurement of N₂O₅ reactivity on ambient particles, *Atmos. Meas. Tech.*,
697 2(1), 231–242, doi:10.5194/amt-2-231-2009, 2009.

698 Bertram, T. H., Kimmel, J. R., Crisp, T. A., Ryder, O. S., Yatavelli, R. L. N.,
699 Thornton, J. A., Cubison, M. J., Gonin, M. and Worsnop, D. R.: A field-deployable,
700 chemical ionization time-of-flight mass spectrometer, *Atmos. Meas. Tech.*, 4(7),
701 1471–1479, doi:10.5194/amt-4-1471-2011, 2011.

702 Bhattarai, H., Saikawa, E., Wan, X., Zhu, H., Ram, K., Gao, S., Kang, S., Zhang, Q.,
703 Zhang, Y., Wu, G., Wang, X., Kawamura, K., Fu, P. and Cong, Z.: Levoglucosan as a
704 tracer of biomass burning: Recent progress and perspectives, *Atmos. Res.*,
705 220(November 2018), 20–33, doi:10.1016/j.atmosres.2019.01.004, 2019.

706 Boyd, C. M., Sanchez, J., Xu, L., Eugene, A. J., Nah, T., Tuet, W. Y., Guzman, M. I.
707 and Ng, N. L.: Secondary organic aerosol formation from the β-pinene+NO₃ system:
708 effect of humidity and peroxy radical fate, *Atmos. Chem. Phys.*, 15(13), 7497–7522,
709 doi:10.5194/acp-15-7497-2015, 2015.

710 Brandt, C. and van Eldik, R.: Transition Metal-Catalyzed Oxidation of Sulfur(IV)
711 Oxides. Atmospheric-Relevant Processes and Mechanisms, *Chem. Rev.*, 95(1), 119–
712 190, doi:10.1021/cr00033a006, 1995.

713 Brege, M., Paglione, M., Gilardoni, S., Decesari, S., Cristina Facchini, M. and

714 Mazzoleni, L. R.: Molecular insights on aging and aqueous-phase processing from
715 ambient biomass burning emissions-influenced Po Valley fog and aerosol, *Atmos.*
716 *Chem. Phys.*, 18(17), 13197–13214, doi:10.5194/acp-18-13197-2018, 2018.

717 Le Breton, M., Hallquist, A. M., Pathak, R. K., Simpson, D., Wang, Y., Johansson, J.,
718 Zheng, J., Yang, Y., Shang, D., Wang, H., Liu, Q., Chan, C., Wang, T., Bannan, T. J.,
719 Priestley, M., Percival, C. J., Shallcross, D. E., Lu, K., Guo, S., Hu, M. and Hallquist,
720 M.: Chlorine oxidation of VOCs at a semi-rural site in Beijing: significant chlorine
721 liberation from ClNO₂ and subsequent gas- and particle-phase Cl-VOC production,
722 *Atmos. Chem. Phys.*, 18(17), 13013–13030, doi:10.5194/acp-18-13013-2018, 2018a.

723 Le Breton, M., Wang, Y., Hallquist, Å. M., Pathak, R. K., Zheng, J., Yang, Y., Shang,
724 D., Glasius, M., Bannan, T. J., Liu, Q., Chan, C. K., Percival, C. J., Zhu, W., Lou, S.,
725 Topping, D., Wang, Y., Yu, J., Lu, K., Guo, S., Hu, M. and Hallquist, M.: Online gas-
726 and particle-phase measurements of organosulfates, organosulfonates and nitrooxy
727 organosulfates in Beijing utilizing a FIGAERO ToF-CIMS, *Atmos. Chem. Phys.*,
728 18(14), 10355–10371, doi:10.5194/acp-18-10355-2018, 2018b.

729 Le Breton, M., Psichoudaki, M., Hallquist, M., Watne, Å. K., Lutz, A. and Hallquist,
730 Å. M.: Application of a FIGAERO ToF CIMS for on-line characterization of real-
731 world fresh and aged particle emissions from buses, *Aerosol Sci. Technol.*, 53(3),
732 244–259, doi:10.1080/02786826.2019.1566592, 2019.

733 Canagaratna, M. R., Jimenez, J. L., Kroll, J. H., Chen, Q., Kessler, S. H., Massoli, P.
734 and Ruiz, L. H.: Elemental ratio measurements of organic compounds using aerosol
735 mass spectrometry: characterization, improved calibration, and implications, *Atmos.*
736 *Chem. Phys.*, 15, 253–272, doi:10.5194/acp-15-253-2015, 2015.

737 Capouet, M. and Müller, J. F.: A group contribution method for estimating the vapour
738 pressures of α -pinene oxidation products, *Atmos. Chem. Phys.*, 6(6), 1455–1467,
739 doi:10.5194/acp-6-1455-2006, 2006.

740 Carlton, A. G., Turpin, B. J., Altieri, K. E., Seitzinger, S., Reff, A., Lim, H.-J. and
741 Ervens, B.: Atmospheric oxalic acid and SOA production from glyoxal: Results of
742 aqueous photooxidation experiments, *Atmos. Environ.*, 41(35), 7588–7602,
743 doi:10.1016/j.atmosenv.2007.05.035, 2007.

744 Carslaw, N.: A mechanistic study of limonene oxidation products and pathways
745 following cleaning activities, *Atmos. Environ.*, 80, 507–513,
746 doi:<https://doi.org/10.1016/j.atmosenv.2013.08.034>, 2013.

747 Chen, H. and Finlayson-Pitts, B. J.: New Particle Formation from Methanesulfonic
748 Acid and Amines/Ammonia as a Function of Temperature, *Environ. Sci. Technol.*,
749 51(1), 243–252, doi:10.1021/acs.est.6b04173, 2017.

750 Chen, J., Wenger, J. C. and Venables, D. S.: Near-Ultraviolet Absorption Cross
751 Sections of Nitrophenols and Their Potential Influence on Tropospheric Oxidation
752 Capacity, *J. Phys. Chem. A*, 115(44), 12235–12242, doi:10.1021/jp206929r, 2011.

753 Cubison, M. J., Ortega, A. M., Hayes, P. L., Farmer, D. K., Day, D., Lechner, M. J.,
754 Brune, W. H., Apel, E., Diskin, G. S., Fisher, J. A., Fuelberg, H. E., Hecobian, A.,
755 Knapp, D. J., Mikoviny, T., Riemer, D., Sachse, G. W., Sessions, W., Weber, R. J.,
756 Weinheimer, A. J., Wisthaler, A. and Jimenez, J. L.: Effects of aging on organic
757 aerosol from open biomass burning smoke in aircraft and laboratory studies, *Atmos.*
758 *Chem. Phys.*, 11(23), 12049–12064, doi:10.5194/acp-11-12049-2011, 2011.

759 D’Ambro, E. L., Lee, B. H., Liu, J., Shilling, J. E., Gaston, C. J., Lopez-Hilfiker, F.
760 D., Schobesberger, S., Zaveri, R. A., Mohr, C., Lutz, A., Zhang, Z., Gold, A., Surratt,
761 J. D., Rivera-Rios, J. C., Keutsch, F. N. and Thornton, J. A.: Molecular composition
762 and volatility of isoprene photochemical oxidation secondary organic aerosol under
763 low- and high-NO_x conditions, *Atmos. Chem. Phys.*, 17(1), 159–174,
764 doi:10.5194/acp-17-159-2017, 2017.

765 D’Ambro, E. L., Schobesberger, S., Zaveri, R. A., Shilling, J. E., Lee, B. H., Lopez-
766 Hilfiker, F. D., Mohr, C. and Thornton, J.: Isothermal evaporation of α -pinene
767 ozonolysis SOA: volatility, phase state, and oligomeric composition, *ACS Earth Sp.*
768 *Chem.*, [acsearchspacechem.8b00084](https://doi.org/10.1021/acsearchspacechem.8b00084), doi:10.1021/acsearchspacechem.8b00084, 2018.

769 Edwards, P. M., Brown, S. S., Roberts, J. M., Ahmadov, R., Banta, R. M., DeGouw,
770 J. A., Dubé, W. P., Field, R. A., Flynn, J. H., Gilman, J. B., Graus, M., Helmig, D.,
771 Koss, A., Langford, A. O., Lefer, B. L., Lerner, B. M., Li, R., Li, S. M., McKeen, S.
772 A., Murphy, S. M., Parrish, D. D., Senff, C. J., Soltis, J., Stutz, J., Sweeney, C.,
773 Thompson, C. R., Trainer, M. K., Tsai, C., Veres, P. R., Washenfelder, R. A.,

774 Warneke, C., Wild, R. J., Young, C. J., Yuan, B. and Zamora, R.: High winter ozone
775 pollution from carbonyl photolysis in an oil and gas basin, *Nature*, 514(7522), 351–
776 354, doi:10.1038/nature13767, 2014.

777 Eger, P. G., Schuladen, J., Sobanski, N., Fischer, H., Karu, E., Williams, J., Riva, M.,
778 Zha, Q., Ehn, M., Quéléver, L. L. J., Schallhart, S., Lelieveld, J. and Crowley, J. N.:
779 Pyruvic acid in the boreal forest: gas-phase mixing ratios and impact on radical
780 chemistry, *Atmos. Chem. Phys.*, 20(6), 3697–3711, doi:10.5194/acp-20-3697-2020,
781 2020.

782 Eisele, F. L. and Tanner, D. J.: Measurement of the gas phase concentration of
783 H₂SO₄ and methane sulfonic acid and estimates of H₂SO₄ production and loss in the
784 atmosphere, *J. Geophys. Res. Atmos.*, 98(D5), 9001–9010, doi:10.1029/93JD00031,
785 1993.

786 Fang, W., Gong, L. and Sheng, L.: Online analysis of secondary organic aerosols
787 from OH-initiated photooxidation and ozonolysis of α -pinene, β -pinene, Δ^3 -carene
788 and d-limonene by thermal desorption-photoionisation aerosol mass spectrometry,
789 *Environ. Chem.*, 14(2), 75–90, doi:10.1071/EN16128, 2017.

790 Faxon, C., Hammes, J., Pathak, R. K. and Hallquist, M.: Characterization of organic
791 nitrate constituents of secondary organic aerosol (SOA) from nitrate-radical-initiated
792 oxidation of limonene using High-Resolution Chemical Ionization Mass
793 Spectrometry, *Atmos. Chem. Phys.*, 18, 5467–5481, doi:10.5194/acp-2017-584, 2018.

794 Fisher, J. A., Jacob, D. J., Travis, K. R., Kim, P. S., Marais, E. A., Chan Miller, C.,
795 Yu, K., Zhu, L., Yantosca, R. M. and Sulprizio, M. P.: Organic Nitrate Chemistry and
796 its Implications for Nitrogen Budgets in an Isoprene- and Monoterpene-Rich
797 Atmosphere: Constraints from Aircraft (SEAC4RS) and Ground-Based (SOAS)
798 Observations in the Southeast US, *Atmos. Chem. Phys.*, 16, 5969 [online] Available
799 from: <https://www.atmos-chem-phys.net/16/5969/2016/acp-16-5969-2016.pdf>, 2016.

800 Fountoukis, C. and Nenes, A.: ISORROPIA II: a computationally efficient
801 thermodynamic equilibrium model for K⁺–Ca²⁺–Mg²⁺–NH₄⁺–Na⁺–SO₄²⁻–NO₃⁻–
802 Cl⁻–H₂O aerosols, *Atmos. Chem. Phys.*, 7(17), 4639–4659, doi:10.5194/acp-7-
803 4639-2007, 2007.

804 Fry, J. L., Draper, D. C., Zarzana, K. J., Campuzano-Jost, P., Day, D. A., Jimenez, J.
805 L., Brown, S. S., Cohen, R. C., Kaser, L., Hansel, A., Cappellin, L., Karl, T., Hodzic
806 Roux, A., Turnipseed, A., Cantrell, C., Lefer, B. L., Grossberg, N., Farmer, D. K. and
807 Jimenez, J. L.: Observations of gas- and aerosol-phase organic nitrates at BEACHON-
808 RoMBAS 2011, *Atmos. Chem. Phys.*, 13(17), 8585–8605, doi:10.5194/acp-13-8585-
809 2013, 2013.

810 Galloway, M. M., Chhabra, P. S., Chan, A. W. H., Surratt, J. D., Flagan, R. C.,
811 Seinfeld, J. H. and Keutsch, F. N.: Glyoxal uptake on ammonium sulphate seed
812 aerosol: reaction products and reversibility of uptake under dark and irradiated
813 conditions, *Atmos. Chem. Phys.*, 9(10), 3331–3345, doi:10.5194/acp-9-3331-2009,
814 2009.

815 Gaston, C. J., Lopez-Hilfiker, F. D., Whybrew, L. E., Hadley, O., McNair, F., Gao,
816 H., Jaffe, D. A. and Thornton, J. A.: Online molecular characterization of fine
817 particulate matter in Port Angeles, WA: Evidence for a major impact from residential
818 wood smoke, *Atmos. Environ.*, 138, 99–107, doi:10.1016/j.atmosenv.2016.05.013,
819 2016.

820 Glasius, M., Lahaniati, M., Calogirou, A., Di Bella, D., Jensen, N. R., Hjorth, J.,
821 Kotzias, D. and Larsen, B. R.: Carboxylic acids in secondary aerosols from oxidation
822 of cyclic monoterpenes by ozone, *Environ. Sci. Technol.*, 34(6), 1001–1010,
823 doi:10.1021/es990445r, 2000.

824 Gondwe, M., Krol, M., Gieskes, W., Klaassen, W. and de Baar, H.: The contribution
825 of ocean-leaving DMS to the global atmospheric burdens of DMS, MSA, SO₂, and
826 NSS SO₄⁼, *Global Biogeochem. Cycles*, 17(2), doi:10.1029/2002GB001937, 2003.

827 de Gouw, J. A., Middlebrook, A. M., Warneke, C., Goldan, P. D., Kuster, W. C.,
828 Roberts, J. M., Fehsenfeld, F. C., Worsnop, D. R., Canagaratna, M. R., Pszenny, A.
829 A. P., Keene, W. C., Marchewka, M., Bertman, S. B. and Bates, T. S.: Budget of
830 organic carbon in a polluted atmosphere: Results from the New England Air Quality
831 Study in 2002, *J. Geophys. Res. D Atmos.*, 110(16), 1–22,
832 doi:10.1029/2004JD005623, 2005.

833 de Gouw, J. A., Gilman, J. B., Kim, S. W., Alvarez, S. L., Dusanter, S., Graus, M.,

834 Griffith, S. M., Isaacman-VanWertz, G., Kuster, W. C., Lefer, B. L., Lerner, B. M.,
835 McDonald, B. C., Rappenglück, B., Roberts, J. M., Stevens, P. S., Stutz, J., Thalman,
836 R., Veres, P. R., Volkamer, R., Warneke, C., Washenfelder, R. A. and Young, C. J.:
837 Chemistry of Volatile Organic Compounds in the Los Angeles Basin: Formation of
838 Oxygenated Compounds and Determination of Emission Ratios, *J. Geophys. Res.*
839 *Atmos.*, 123(4), 2298–2319, doi:10.1002/2017JD027976, 2018.

840 Guo, H., Xu, L., Bougiatioti, A., Cerully, K. M., Capps, S. L., Hite, J. R., Carlton, A.
841 G., Lee, S. H., Bergin, M. H., Ng, N. L., Nenes, A. and Weber, R. J.: Fine-particle
842 water and pH in the southeastern United States, *Atmos. Chem. Phys.*, 15(9), 5211–
843 5228, doi:10.5194/acp-15-5211-2015, 2015.

844 Hallquist, M., Wenger, J. C., Baltensperger, U., Rudich, Y., Simpson, D., Claeys, M.,
845 Dommen, J., Donahue, N. M., George, C., Goldstein, a. H., Hamilton, J. F.,
846 Herrmann, H., Hoffmann, T., Iinuma, Y., Jang, M., Jenkin, M. E., Jimenez, J. L.,
847 Kiendler-Scharr, a., Maenhaut, W., McFiggans, G., Mentel, T. F., Monod, a.,
848 Prévôt, a. S. H., Seinfeld, J. H., Surratt, J. D., Szmigielski, R. and Wildt, J.: The
849 formation, properties and impact of secondary organic aerosol: current and emerging
850 issues, *Atmos. Chem. Phys.*, 9(14), 5155–5236, doi:10.5194/acp-9-5155-2009, 2009.

851 Hammes, J., Lutz, A., Mentel, T., Faxon, C. and Hallquist, M.: Carboxylic acids from
852 limonene oxidation by ozone and hydroxyl radicals: insights into mechanisms derived
853 using a FIGAERO-CIMS, *Atmos. Chem. Phys.*, 19(20), 13037–13052,
854 doi:10.5194/acp-19-13037-2019, 2019.

855 Harrison, M. A. J., Barra, S., Borghesi, D., Vione, D., Arsene, C. and Iulian Olariu,
856 R.: Nitrated phenols in the atmosphere: a review, *Atmos. Environ.*, 39(2), 231–248,
857 doi:https://doi.org/10.1016/j.atmosenv.2004.09.044, 2005.

858 He, Q.-F., Ding, X., Wang, X.-M., Yu, J.-Z., Fu, X.-X., Liu, T.-Y., Zhang, Z., Xue, J.,
859 Chen, D.-H., Zhong, L.-J. and Donahue, N. M.: Organosulfates from Pinene and
860 Isoprene over the Pearl River Delta, South China: Seasonal Variation and Implication
861 in Formation Mechanisms, *Environ. Sci. Technol.*, 48(16), 9236–9245,
862 doi:10.1021/es501299v, 2014.

863 Heald, C. L., Kroll, J. H., Jimenez, J. L., Docherty, K. S., Decarlo, P. F., Aiken, A. C.,

864 Chen, Q., Martin, S. T., Farmer, D. K. and Artaxo, P.: A simplified description of the
865 evolution of organic aerosol composition in the atmosphere, *Geophys. Res. Lett.*,
866 37(8), doi:10.1029/2010GL042737, 2010.

867 Hodzic, A., Jimenez, J. L., Madronich, S., Canagaratna, M. R., Decarlo, P. F.,
868 Kleinman, L. and Fast, J.: Modeling organic aerosols in a megacity: Potential
869 contribution of semi-volatile and intermediate volatility primary organic compounds
870 to secondary organic aerosol formation, *Atmos. Chem. Phys.*, 10(12), 5491–5514,
871 doi:10.5194/acp-10-5491-2010, 2010.

872 Hu, W., Hu, M., Hu, W., Jimenez, J. L., Yuan, B., Chen, W., Wang, M., Wu, Y.,
873 Chen, C., Wang, Z., Peng, J., Zeng, L. and Shao, M.: Chemical composition, sources,
874 and aging process of submicron aerosols in Beijing: Contrast between summer and
875 winter, *J. Geophys. Res. Atmos.*, 121(4), 1955–1977,
876 doi:10.1002/2015JD024020. Received, 2016.

877 Hu, W., Day, D. A., Campuzano-Jost, P., Nault, B. A., Park, T., Lee, T., Croteau, P.,
878 Canagaratna, M. R., Jayne, J. T., Worsnop, D. R. and Jimenez, J. L.: Evaluation of the
879 new capture vaporizer for aerosol mass spectrometers: Characterization of organic
880 aerosol mass spectra, *Aerosol Sci. Technol.*, 52(7), 725–739,
881 doi:10.1080/02786826.2018.1454584, 2018.

882 Huang, R.-J., Cao, J., Chen, Y., Yang, L., Shen, J., You, Q., Wang, K., Lin, C., Xu,
883 W., Gao, B., Li, Y., Chen, Q., Hoffmann, T., O’Dowd, C. D., Bilde, M. and Glasius,
884 M.: Organosulfates in atmospheric aerosol: synthesis and quantitative analysis of
885 PM_{2.5} from Xi’an, northwestern China, *Atmos. Meas. Tech.*, 11(6), 3447–3456,
886 doi:10.5194/amt-11-3447-2018, 2018.

887 Huang, R. J., Zhang, Y., Bozzetti, C., Ho, K. F., Cao, J. J., Han, Y., Daellenbach, K.
888 R., Slowik, J. G., Platt, S. M., Canonaco, F., Zotter, P., Wolf, R., Pieber, S. M., Bruns,
889 E. A., Crippa, M., Ciarelli, G., Piazzalunga, A., Schwikowski, M., Abbaszade, G.,
890 Schnelle-Kreis, J., Zimmermann, R., An, Z., Szidat, S., Baltensperger, U., El Haddad,
891 I. and Prévôt, A. S. H.: High secondary aerosol contribution to particulate pollution
892 during haze events in China, *Nature*, 514(7521), 218–222, doi:10.1038/nature13774,
893 2015.

894 Huang, W., Saathoff, H., Shen, X., Ramisetty, R., Leisner, T. and Mohr, C.: Chemical
895 Characterization of Highly Functionalized Organonitrates Contributing to Night-Time
896 Organic Aerosol Mass Loadings and Particle Growth, *Environ. Sci. Technol.*, 53(3),
897 1165–1174, doi:10.1021/acs.est.8b05826, 2019.

898 Hunter, J. F., Day, D. A., Palm, B. B., Yatavelli, R. L. N., Chan, A. W. H., Kaser, L.,
899 Cappellin, L., Hayes, P. L., Cross, E. S., Carrasquillo, A. J., Campuzano-Jost, P.,
900 Stark, H., Zhao, Y., Hohaus, T., Smith, J. N., Hansel, A., Karl, T., Goldstein, A. H.,
901 Guenther, A., Worsnop, D. R., Thornton, J. A., Heald, C. L., Jimenez, J. L. and Kroll,
902 J. H.: Comprehensive characterization of atmospheric organic carbon at a forested
903 site, *Nat. Geosci.*, 10(10), 748–753, doi:10.1038/NGEO3018, 2017.

904 Hyttinen, N., Otkjær, R. V., Iyer, S., Kjaergaard, H. G., Rissanen, M. P., Wennberg,
905 P. O. and Kurtén, T.: Computational Comparison of Different Reagent Ions in the
906 Chemical Ionization of Oxidized Multifunctional Compounds, *J. Phys. Chem. A*,
907 122(1), 269–279, doi:10.1021/acs.jpca.7b10015, 2018.

908 Isaacman-VanWertz, G., Massoli, P., O’Brien, R., Lim, C., Franklin, J., Moss, J.,
909 Hunter, J., Nowak, J., Canagaratna, M., Misztal, P., Arata, C., Roscioli, J., Herndon,
910 S., Onasch, T., Lambe, A., Jayne, J., Su, L., Knopf, D., Goldstein, A., Worsnop, D.
911 and Kroll, J.: Chemical evolution of atmospheric organic carbon over multiple
912 generations of oxidation, *Nat. Chem.*, 10(4), 462–468, doi:10.1038/s41557-018-0002-
913 2, 2018.

914 Iyer, S., Lopez-Hilfiker, F., Lee, B. H., Thornton, J. A. and Kurtén, T.: Modeling the
915 Detection of Organic and Inorganic Compounds Using Iodide-Based Chemical
916 Ionization, *J. Phys. Chem. A*, 120(4), 576–587, doi:10.1021/acs.jpca.5b09837, 2016.

917 Jacobs, M. I., Burke, W. J. and Elrod, M. J.: Kinetics of the Reactions of Isoprene-
918 Derived Hydroxynitrates: Gas Phase Epoxide Formation and Solution Phase
919 Hydrolysis, *Atmos. Chem. Phys.*, 14, 8933, 2014.

920 Jenkin, M. E., Saunders, S. M., Wagner, V. and Pilling, M. J.: Protocol for the
921 development of the Master Chemical Mechanism, MCM v3 (Part B): tropospheric
922 degradation of aromatic volatile organic compounds, *Atmos. Chem. Phys.*, 3(1), 181–
923 193, doi:10.5194/acp-3-181-2003, 2003.

924 Karl, T., Striednig, M., Graus, M., Hammerle, A. and Wohlfahrt, G.: Urban flux
925 measurements reveal a large pool of oxygenated volatile organic compound
926 emissions, *Proc. Natl. Acad. Sci.*, 201714715, doi:10.1073/pnas.1714715115, 2018.

927 Kawamura, K. and Bikkina, S.: A review of dicarboxylic acids and related
928 compounds in atmospheric aerosols: Molecular distributions, sources and
929 transformation, *Atmos. Res.*, 170, 140–160,
930 doi:<https://doi.org/10.1016/j.atmosres.2015.11.018>, 2016.

931 Kawamura, K., Kasukabe, H. and Barrie, L. A.: Source and reaction pathways of
932 dicarboxylic acids, ketoacids and dicarbonyls in arctic aerosols: One year of
933 observations, *Atmos. Environ.*, 30(10), 1709–1722, doi:[https://doi.org/10.1016/1352-](https://doi.org/10.1016/1352-2310(95)00395-9)
934 [2310\(95\)00395-9](https://doi.org/10.1016/1352-2310(95)00395-9), 1996.

935 Kong, X., Salvador, C. M., Carlsson, S., Pathak, R., Davidsson, K. O., Le Breton, M.,
936 Gaita, S. M., Mitra, K., Hallquist, Å. M., Hallquist, M. and Pettersson, J. B. C.:
937 Molecular characterization and optical properties of primary emissions from a
938 residential wood burning boiler, *Sci. Total Environ.*, 754, 142143,
939 doi:<https://doi.org/10.1016/j.scitotenv.2020.142143>, 2021.

940 Krechmer, J. E., Pagonis, D., Ziemann, P. J. and Jimenez, J. L.: Quantification of Gas-
941 Wall Partitioning in Teflon Environmental Chambers Using Rapid Bursts of Low-
942 Volatility Oxidized Species Generated in Situ, *Environ. Sci. Technol.*, 50(11), 5757–
943 5765, doi:10.1021/acs.est.6b00606, 2016.

944 Kroll, J. H. and Seinfeld, J. H.: Chemistry of secondary organic aerosol: Formation
945 and evolution of low-volatility organics in the atmosphere, *Atmos. Environ.*, 42(16),
946 3593–3624, doi:10.1016/j.atmosenv.2008.01.003, 2008.

947 Lambe, A. T., Onasch, T. B., Croasdale, D. R., Wright, J. P., Martin, A. T., Franklin,
948 J. P., Massoli, P., Kroll, J. H., Canagaratna, M. R., Brune, W. H., Worsnop, D. R. and
949 Davidovits, P.: Transitions from functionalization to fragmentation reactions of
950 laboratory Secondary Organic Aerosol (SOA) generated from the OH oxidation of
951 alkane precursors, *Environ. Sci. Technol.*, 46(10), 5430–5437,
952 doi:10.1021/es300274t, 2012.

953 Larsen, B. R., Di Bella, D., Glasius, M., Winterhalter, R., Jensen, N. R. and Hjorth, J.:

954 Gas-phase OH oxidation of monoterpenes: Gaseous and particulate products, J.
955 Atmos. Chem., 38(3), 231–276, doi:10.1023/A:1006487530903, 2001.

956 Lee, B. H., Lopez-Hilfiker, F. D., Mohr, C., Kurtén, T., Worsnop, D. R. and
957 Thornton, J. A.: An iodide-adduct high-resolution time-of-flight chemical-ionization
958 mass spectrometer: Application to atmospheric inorganic and organic compounds,
959 Environ. Sci. Technol., 48(11), 6309–6317, doi:10.1021/es500362a, 2014.

960 Lee, B. H., Mohr, C., Lopez-Hilfiker, F. D., Lutz, A., Hallquist, M., Lee, L., Romer,
961 P., Cohen, R. C., Iyer, S., Kurtén, T., Hu, W., Day, D. A., Campuzano-Jost, P.,
962 Jimenez, J. L., Xu, L., Ng, N. L., Guo, H., Weber, R. J., Wild, R. J., Brown, S. S.,
963 Koss, A., de Gouw, J., Olson, K., Goldstein, A. H., Seco, R., Kim, S., McAvey, K.,
964 Shepson, P. B., Starn, T., Baumann, K., Edgerton, E. S., Liu, J., Shilling, J. E., Miller,
965 D. O., Brune, W., Schobesberger, S., D’Ambro, E. L. and Thornton, J. A.: Highly
966 functionalized organic nitrates in the southeast United States: Contribution to
967 secondary organic aerosol and reactive nitrogen budgets, Proc. Natl. Acad. Sci.,
968 113(6), 1516–1521, doi:10.1073/pnas.1508108113, 2016.

969 Lee, B. H., Lopez-hilfiker, F. D., Veres, P. R., Mcduffie, E. E., Fibiger, D. L.,
970 Tamara, L. and Thornton, J. A.: Flight deployment of a high-resolution time-of-flight
971 chemical ionization mass spectrometer : observations of reactive halogen and nitrogen
972 oxide species, , doi:10.1029/2017JD028082, 2018a.

973 Lee, B. H., Lopez-Hilfiker, F. D., D’Ambro, E. L., Zhou, P., Boy, M., Petäjä, T., Hao,
974 L., Virtanen, A. and Thornton, J. A.: Semi-volatile and highly oxygenated gaseous
975 and particulate organic compounds observed above a boreal forest canopy, Atmos.
976 Chem. Phys., 18(15), 11547–11562, doi:10.5194/acp-18-11547-2018, 2018b.

977 Li, T., Wang, Z., Yuan, B., Ye, C., Lin, Y., Wang, S., Sha, Q., Yuan, Z., Zheng, J. and
978 Shao, M.: Emissions of carboxylic acids, hydrogen cyanide (HCN) and isocyanic acid
979 (HNCO) from vehicle exhaust, Atmos. Environ., 247, 118218,
980 doi:https://doi.org/10.1016/j.atmosenv.2021.118218, 2021.

981 Liao, J., Froyd, K. D., Murphy, D. M., Keutsch, F. N., Yu, G., Wennberg, P. O., St
982 Clair, J. M., Crouse, J. D., Wisthaler, A., Mikoviny, T., Jimenez, J. L., Campuzano-
983 Jost, P., Day, D. A., Hu, W., Ryerson, T. B., Pollack, I. B., Peischl, J., Anderson, B.

984 E., Ziemba, L. D., Blake, D. R., Meinardi, S. and Diskin, G.: Airborne measurements
985 of organosulfates over the continental U.S, *J. Geophys. Res. Atmos.* JGR, 120(7),
986 2990–3005, doi:10.1002/2014JD022378, 2015.

987 Lim, H.-J., Carlton, A. G. and Turpin, B. J.: Isoprene Forms Secondary Organic
988 Aerosol through Cloud Processing: Model Simulations, *Environ. Sci. Technol.*,
989 39(12), 4441–4446, doi:10.1021/es048039h, 2005.

990 Liu, C., Deng, X., Zhu, B. and Yin, C.: Characteristics of GSR of China’s three major
991 economic regions in the past 10 years and its relationship with O₃ and PM_{2.5}, *China*
992 *Environ. Sci.*, 38(08), 2820–2829, doi:10.19674/j.cnki.issn1000-6923.2018.0295,
993 2018.

994 Liu, X., Qu, H., Huey, L. G., Wang, Y., Sjostedt, S., Zeng, L., Lu, K., Wu, Y., Hu,
995 M., Shao, M., Zhu, T. and Zhang, Y.: High Levels of Daytime Molecular Chlorine
996 and Nitryl Chloride at a Rural Site on the North China Plain, *Environ. Sci. Technol.*,
997 51(17), 9588–9595, doi:10.1021/acs.est.7b03039, 2017.

998 Liu, Z., Wang, Y., Gu, D., Zhao, C., Huey, L. G., Stickel, R., Liao, J., Shao, M., Zhu,
999 T., Zeng, L., Amoroso, A., Costabile, F., Chang, C. C. and Liu, S. C.: Summertime
1000 photochemistry during CAREBeijing-2007: RO_xbudgets and O₃ formation, *Atmos.*
1001 *Chem. Phys.*, 12(16), 7737–7752, doi:10.5194/acp-12-7737-2012, 2012.

1002 Lopez-Hilfiker, F. D., Mohr, C., Ehn, M., Rubach, F., Kleist, E., Wildt, J., Mentel, T.
1003 F., Lutz, A., Hallquist, M., Worsnop, D. and Thornton, J. A.: A novel method for
1004 online analysis of gas and particle composition: description and evaluation of a Filter
1005 Inlet for Gases and AEROSols (FIGAERO), *Atmos. Meas. Tech.*, 7(4), 983–1001,
1006 doi:10.5194/amt-7-983-2014, 2014.

1007 Lopez-Hilfiker, F. D., Mohr, C., Ehn, M., Rubach, F., Kleist, E., Wildt, J., Mentel, T.
1008 F. and Carrasquillo, A. J.: Phase partitioning and volatility of secondary organic
1009 aerosol components formed from α -pinene ozonolysis and OH oxidation : the
1010 importance of accretion products and other low volatility compounds, *Atmos. Chem.*
1011 *Phys.*, 15, 7765–7776, doi:10.5194/acp-15-7765-2015, 2015.

1012 Lopez-Hilfiker, F. D., Iyer, S., Mohr, C., Lee, B. H., Ambro, E. L. D., Kurtén, T. and
1013 Thornton, J. A.: Constraining the sensitivity of iodide adduct chemical ionization

1014 mass spectrometry to multifunctional organic molecules using the collision limit and
1015 thermodynamic stability of iodide ion adducts, *Atmos. Meas. Tech.*, **9**, 1505–1512,
1016 doi:10.5194/amt-9-1505-2016, 2016.

1017 Massoli, P., Stark, H., Canagaratna, M. R., Krechmer, J. E., Xu, L., Ng, N. L.,
1018 Mauldin, R. L., Yan, C., Kimmel, J., Misztal, P. K., Jimenez, J. L., Jayne, J. T. and
1019 Worsnop, D. R.: Ambient Measurements of Highly Oxidized Gas-Phase Molecules
1020 during the Southern Oxidant and Aerosol Study (SOAS) 2013, *ACS Earth Sp. Chem.*,
1021 **2**(7), 653–672, doi:10.1021/acsearthspacechem.8b00028, 2018.

1022 Mattila, J. M., Brophy, P., Kirkland, J., Hall, S., Ullmann, K., Fischer, E. V., Brown,
1023 S., McDuffie, E., Tevlin, A. and Farmer, D. K.: Tropospheric sources and sinks of
1024 gas-phase acids in the Colorado Front Range, *Atmos. Chem. Phys.*, **18**(16), 12315–
1025 12327, doi:10.5194/acp-18-12315-2018, 2018.

1026 Mehra, A., Wang, Y., Krechmer, J. E., Lambe, A., Majluf, F., Morris, M. A.,
1027 Priestley, M., Bannan, T. J., Bryant, D. J., Pereira, K. L., Hamilton, J. F., Rickard, A.
1028 R., Newland, M. J., Stark, H., Croteau, P., Jayne, J. T., Worsnop, D. R., Canagaratna,
1029 M. R., Wang, L. and Coe, H.: Evaluation of the chemical composition of gas- and
1030 particle-phase products of aromatic oxidation, *Atmos. Chem. Phys.*, **20**(16), 9783–
1031 9803, doi:10.5194/acp-20-9783-2020, 2020.

1032 Mellouki, A., Wallington, T. J. and Chen, J.: Atmospheric Chemistry of Oxygenated
1033 Volatile Organic Compounds: Impacts on Air Quality and Climate, *Chem. Rev.*,
1034 **115**(10), 3984–4014, doi:10.1021/cr500549n, 2015.

1035 Mohr, C., Lopez-Hilfiker, F. D., Zotter, P., Prévôt, A. S. H., Xu, L., Ng, N. L.,
1036 Herndon, S. C., Williams, L. R., Franklin, J. P., Zahniser, M. S., Worsnop, D. R.,
1037 Knighton, W. B., Aiken, A. C., Gorkowski, K. J., Dubey, M. K., Allan, J. D. and
1038 Thornton, J. A.: Contribution of Nitrated Phenols to Wood Burning Brown Carbon
1039 Light Absorption in Detling, United Kingdom during Winter Time, *Environ. Sci.*
1040 *Technol.*, **47**(12), 6316–6324, doi:10.1021/es400683v, 2013.

1041 Mutzel, A., Poulain, L., Berndt, T., Iinuma, Y., Rodigast, M., Böge, O., Richters, S.,
1042 Spindler, G., Sipilä, M., Jokinen, T., Kulmala, M. and Herrmann, H.: Highly
1043 Oxidized Multifunctional Organic Compounds Observed in Tropospheric Particles: A

1044 Field and Laboratory Study, *Environ. Sci. Technol.*, 49(13), 7754–7761,
1045 doi:10.1021/acs.est.5b00885, 2015.

1046 Mutzel, A., Rodigast, M., Iinuma, Y., Böge, O. and Herrmann, H.: Monoterpene SOA
1047 - Contribution of first-generation oxidation products to formation and chemical
1048 composition, *Atmos. Environ.*, 130, 136–144, doi:10.1016/j.atmosenv.2015.10.080,
1049 2016.

1050 Nah, T., Sanchez, J., Boyd, C. M. and Ng, N. L.: Photochemical Aging of α -pinene
1051 and β -pinene Secondary Organic Aerosol formed from Nitrate Radical Oxidation,
1052 *Environ. Sci. Technol.*, 50(1), 222–231, doi:10.1021/acs.est.5b04594, 2016.

1053 Nannoolal, Y., Rarey, J. and Ramjugernath, D.: Estimation of pure component
1054 properties Part 3. Estimation of the vapor pressure of non-electrolyte organic
1055 compounds via group contributions and group interactions, *Fluid Phase Equilib.*,
1056 269(1–2), 117–133, doi:10.1016/j.fluid.2008.04.020, 2008.

1057 Ng, N. L., Brown, S. S., Archibald, A. T., Atlas, E., Cohen, R. C., Crowley, J. N.,
1058 Day, D. A., Donahue, N. M., Fry, J. L., Fuchs, H., Griffin, R. J., Guzman, M. I.,
1059 Herrmann, H., Hodzic, A., Iinuma, Y., Jimenez, J. L., Kiendler-Scharr, A., Lee, B. H.,
1060 Luecken, D. J., Mao, J., McLaren, R., Mutzel, A., Osthoff, H. D., Ouyang, B.,
1061 Picquet-Varrault, B., Platt, U., Pye, H. O. T., Rudich, Y., Schwantes, R. H., Shiraiwa,
1062 M., Stutz, J., Thornton, J. A., Tilgner, A., Williams, B. J. and Zaveri, R. A.: Nitrate
1063 radicals and biogenic volatile organic compounds: oxidation, mechanisms, and
1064 organic aerosol, *Atmos. Chem. Phys.*, 17(3), 2103–2162, doi:10.5194/acp-17-2103-
1065 2017, 2017.

1066 Noelscher, A. C., Yanez-Serrano, A. M., Wolff, S., de Araujo, A. C., Lavric, J. V.,
1067 Kesselmeier, J. and Williams, J.: Unexpected seasonality in quantity and composition
1068 of Amazon rainforest air reactivity, *Nat. Commun.*, 7, doi:10.1038/ncomms10383,
1069 2016.

1070 Osthoff, H. D., Roberts, J. M., Ravishankara, A. R., Williams, E. J., Lerner, B. M.,
1071 Sommariva, R., Bates, T. S., Coffman, D., Quinn, P. K., Dibb, J. E., Stark, H.,
1072 Burkholder, J. B., Talukdar, R. K., Meagher, J., Fehsenfeld, F. C. and Brown, S. S.:
1073 High levels of nitryl chloride in the polluted subtropical marine boundary layer, *Nat.*

1074 Geosci., 1(5), 324–328, doi:10.1038/ngeo177, 2008.

1075 Palm, B. B., Liu, X., Jimenez, J. L. and Thornton, J. A.: Performance of a new coaxial
1076 ion-molecule reaction region for low-pressure chemical ionization mass spectrometry
1077 with reduced instrument wall interactions, *Atmos. Meas. Tech.*, 12(11), 5829–5844,
1078 doi:10.5194/amt-12-5829-2019, 2019.

1079 Pankow, J. F. and Asher, W. E.: SIMPOL.1: A simple group contribution method for
1080 predicting vapor pressures and enthalpies of vaporization of multifunctional organic
1081 compounds, *Atmos. Chem. Phys.*, 8(10), 2773–2796, doi:10.5194/acp-8-2773-2008,
1082 2008.

1083 Paulot, F., Crouse, J. D., Kjaergaard, H. G., Kroll, J. H., Seinfeld, J. H. and
1084 Wennberg, P. O.: Isoprene photooxidation: New insights into the production of acids
1085 and organic nitrates, *Atmos. Chem. Phys.*, 9(4), 1479–1501, doi:10.5194/acp-9-1479-
1086 2009, 2009.

1087 Qi, L., Chen, M., Stefenelli, G., Pospisilova, V., Tong, Y., Bertrand, A., Hueglin, C.,
1088 Ge, X., Baltensperger, U., Prévôt, A. S. H. and Slowik, J. G.: Organic aerosol source
1089 apportionment in Zurich using an extractive electrospray ionization time-of-flight
1090 mass spectrometer (EESI-TOF-MS) – Part 2: Biomass burning influences in winter,
1091 *Atmos. Chem. Phys.*, 19(12), 8037–8062, doi:10.5194/acp-19-8037-2019, 2019.

1092 Reyes-Villegas, E., Bannan, T., Le Breton, M., Mehra, A., Priestley, M., Percival, C.,
1093 Coe, H. and Allan, J. D.: Online Chemical Characterization of Food-Cooking Organic
1094 Aerosols: Implications for Source Apportionment, *Environ. Sci. Technol.*, 52(9),
1095 5308–5318, doi:10.1021/acs.est.7b06278, 2018.

1096 Riva, M., Rantala, P., Krechmer, J. E., Peräkylä, O., Zhang, Y., Heikkinen, L.,
1097 Garmash, O., Yan, C., Kulmala, M., Worsnop, D. and Ehn, M.: Evaluating the
1098 performance of five different chemical ionization techniques for detecting gaseous
1099 oxygenated organic species, *Atmos. Meas. Tech.*, 2018(4), 1–39, doi:10.5194/amt-
1100 2018-407, 2019.

1101 Sander, R. and Crutzen, P. J.: Model study indicating halogen activation and ozone
1102 destruction in polluted air masses transported to the sea, *J. Geophys. Res. Atmos.*,
1103 101(D4), 9121–9138, doi:10.1029/95JD03793, 1996.

1104 Schneider, J., Weimer, S., Drewnick, F., Borrmann, S., Helas, G., Gwaze, P., Schmid,
1105 O., Andreae, M. O. and Kirchner, U.: Mass spectrometric analysis and aerodynamic
1106 properties of various types of combustion-related aerosol particles, *Int. J. Mass*
1107 *Spectrom.*, 258(1), 37–49, doi:<https://doi.org/10.1016/j.ijms.2006.07.008>, 2006.

1108 Schwantes, R. H., Teng, A. P., Nguyen, T. B., Coggon, M. M., Crouse, J. D., St
1109 Clair, J. M., Zhang, X., Schilling, K. A., Seinfeld, J. H. and Wennberg, P. O.:
1110 Isoprene NO₃ Oxidation Products from the RO₂ + HO₂ Pathway, *J. Phys. Chem. A*,
1111 119, 10158, 2015.

1112 Schwantes, R. H., Schilling, K. A., McVay, R. C., Lignell, H., Coggon, M. M.,
1113 Zhang, X., Wennberg, P. O. and Seinfeld, J. H.: Formation of highly oxygenated low-
1114 volatility products from cresol oxidation, *Atmos. Chem. Phys.*, 17(5), 3453–3474,
1115 doi:10.5194/acp-17-3453-2017, 2017.

1116 Schwantes, R. H., Emmons, L. K., Orlando, J. J., Barth, M. C., Tyndall, G. S., Hall, S.
1117 R., Ullmann, K., St. Clair, J. M., Blake, D. R., Wisthaler, A. and Paul V. Bui, T.:
1118 Comprehensive isoprene and terpene gas-phase chemistry improves simulated surface
1119 ozone in the southeastern US, *Atmos. Chem. Phys.*, 20(6), 3739–3776,
1120 doi:10.5194/acp-20-3739-2020, 2020.

1121 Shrivastava, M., Andreae, M. O., Artaxo, P., Barbosa, H. M. J., Berg, L. K., Brito, J.,
1122 Ching, J., Easter, R. C., Fan, J., Fast, J. D., Feng, Z., Fuentes, J. D., Glasius, M.,
1123 Goldstein, A. H., Alves, E. G., Gomes, H., Gu, D., Guenther, A., Jathar, S. H., Kim,
1124 S., Liu, Y., Lou, S., Martin, S. T., McNeill, V. F., Medeiros, A., de Sá, S. S., Shilling,
1125 J. E., Springston, S. R., Souza, R. A. F., Thornton, J. A., Isaacman-VanWertz, G.,
1126 Yee, L. D., Ynoue, R., Zaveri, R. A., Zelenyuk, A. and Zhao, C.: Urban pollution
1127 greatly enhances formation of natural aerosols over the Amazon rainforest, *Nat.*
1128 *Commun.*, 10(1), doi:10.1038/s41467-019-08909-4, 2019.

1129 Simoneit, B. R. T., Schauer, J. J., Nolte, C. G., Oros, D. R., Elias, V. O., Fraser, M.
1130 P., Rogge, W. F. and Cass, G. R.: Levoglucosan, a tracer for cellulose in biomass
1131 burning and atmospheric particles, *Atmos. Environ.*, 33(2), 173–182,
1132 doi:[https://doi.org/10.1016/S1352-2310\(98\)00145-9](https://doi.org/10.1016/S1352-2310(98)00145-9), 1999.

1133 Slusher, D. L., Huey, L. G., Tanner, D. J., Flocke, F. M. and Roberts, J. M.: A thermal

1134 dissociation–chemical ionization mass spectrometry (TD-CIMS) technique for the
1135 simultaneous measurement of peroxyacyl nitrates and dinitrogen pentoxide, *J.*
1136 *Geophys. Res. Atmos.*, 109(D19), doi:10.1029/2004JD004670, 2004.

1137 Stark, H., Yatavelli, R. L. N., Thompson, S. L., Kimmel, J. R., Cubison, M. J.,
1138 Chhabra, P. S., Canagaratna, M. R., Jayne, J. T., Worsnop, D. R. and Jimenez, J. L.:
1139 Methods to extract molecular and bulk chemical information from series of complex
1140 mass spectra with limited mass resolution, *Int. J. Mass Spectrom.*, 389, 26–38,
1141 doi:10.1016/j.ijms.2015.08.011, 2015.

1142 Stark, H., Yatavelli, R. L. N., Thompson, S. L., Kang, H., Krechmer, J. E., Kimmel, J.
1143 R., Palm, B. B., Hu, W., Hayes, P. L., Day, D. A., Campuzano-Jost, P., Canagaratna,
1144 M. R., Jayne, J. T., Worsnop, D. R. and Jimenez, J. L.: Impact of Thermal
1145 Decomposition on Thermal Desorption Instruments: Advantage of Thermogram
1146 Analysis for Quantifying Volatility Distributions of Organic Species, *Environ. Sci.*
1147 *Technol.*, 51(15), 8491–8500, doi:10.1021/acs.est.7b00160, 2017.

1148 Stolzenburg, D., Fischer, L., Vogel, A. L., Heinritzi, M., Schervish, M., Simon, M.,
1149 Wagner, A. C., Dada, L., Ahonen, L. R., Amorim, A., Baccarini, A., Bauer, P. S.,
1150 Baumgartner, B., Bergen, A., Bianchi, F., Breitenlechner, M., Brilke, S., Buenrostro
1151 Mazon, S., Chen, D., Dias, A., Draper, D. C., Duplissy, J., El Haddad, I.,
1152 Finkenzeller, H., Frege, C., Fuchs, C., Garmash, O., Gordon, H., He, X., Helm, J.,
1153 Hofbauer, V., Hoyle, C. R., Kim, C., Kirkby, J., Kontkanen, J., Kürten, A.,
1154 Lampilahti, J., Lawler, M., Lehtipalo, K., Leiminger, M., Mai, H., Mathot, S.,
1155 Mentler, B., Molteni, U., Nie, W., Nieminen, T., Nowak, J. B., Ojdanic, A., Onnela,
1156 A., Passananti, M., Petäjä, T., Quéléver, L. L. J., Rissanen, M. P., Sarnela, N.,
1157 Schallhart, S., Tauber, C., Tomé, A., Wagner, R., Wang, M., Weitz, L., Wimmer, D.,
1158 Xiao, M., Yan, C., Ye, P., Zha, Q., Baltensperger, U., Curtius, J., Dommen, J., Flagan,
1159 R. C., Kulmala, M., Smith, J. N., Worsnop, D. R., Hansel, A., Donahue, N. M.,
1160 Winkler, P. M., Nie, W., Passananti, M., Leiminger, M., Stolzenburg, D., Yan, C.,
1161 Wimmer, D., Buenrostro Mazon, S., Kontkanen, J., Wang, M., Garmash, O., Kulmala,
1162 M., Petäjä, T., Bianchi, F., Chen, D., Nieminen, T., Brilke, S., Nowak, J. B., Duplissy,
1163 J., El Haddad, I., Simon, M., Wagner, A. C., Kürten, A., Smith, J. N., Kim, C., et al.:

1164 Rapid growth of organic aerosol nanoparticles over a wide tropospheric temperature
1165 range, *Proc. Natl. Acad. Sci.*, 115(37), 201807604, doi:10.1073/pnas.1807604115,
1166 2018.

1167 Surratt, J. D., Murphy, S. M., Kroll, J. H., Ng, N. L., Hildebrandt, L., Sorooshian, A.,
1168 Szmigielski, R., Vermeylen, R., Maenhaut, W., Claeys, M., Flagan, R. C. and
1169 Seinfeld, J. H.: Chemical Composition of Secondary Organic Aerosol Formed from
1170 the Photooxidation of Isoprene, *J. Phys. Chem. A*, 110(31), 9665–9690,
1171 doi:10.1021/jp061734m, 2006.

1172 Surratt, J. D., Kroll, J. H., Kleindienst, T. E., Edney, E. O., Claeys, M., Sorooshian,
1173 A., Ng, N. L., Offenberg, J. H., Lewandowski, M., Jaoui, M., Flagan, R. C. and
1174 Seinfeld, J. H.: Evidence for Organosulfates in Secondary Organic Aerosol, *Environ.*
1175 *Sci. Technol.*, 41(2), 517–527, doi:10.1021/es062081q, 2007.

1176 Surratt, J. D., Chan, A. W. H., Eddingsaas, N. C., Chan, M., Loza, C. L., Kwan, A. J.,
1177 Hersey, S. P., Flagan, R. C., Wennberg, P. O. and Seinfeld, J. H.: Reactive
1178 intermediates revealed in secondary organic aerosol formation from isoprene, *Proc.*
1179 *Natl. Acad. Sci.*, 107(15), 6640–6645, doi:10.1073/pnas.0911114107, 2010.

1180 Thornton, J. A., Mohr, C., Schobesberger, S., D’Ambro, E. L., Lee, B. H. and Lopez-
1181 Hilfiker, F. D.: Evaluating Organic Aerosol Sources and Evolution with a Combined
1182 Molecular Composition and Volatility Framework Using the Filter Inlet for Gases and
1183 Aerosols (FIGAERO), *Acc. Chem. Res.*, 53(8), 1415–1426,
1184 doi:10.1021/acs.accounts.0c00259, 2020.

1185 Volkamer, R., Jimenez, J. L., San Martini, F., Dzepina, K., Zhang, Q., Salcedo, D.,
1186 Molina, L. T., Worsnop, D. R. and Molina, M. J.: Secondary organic aerosol
1187 formation from anthropogenic air pollution: Rapid and higher than expected,
1188 *Geophys. Res. Lett.*, 33(17), doi:10.1029/2006GL026899, 2006.

1189 Wang, H., Gao, Y., Wang, S., Wu, X., Liu, Y., Li, X., Huang, D., Lou, S., Wu, Z.,
1190 Guo, S., Jing, S., Li, Y., Huang, C., Tyndall, G. S., Orlando, J. J. and Zhang, X.:
1191 Atmospheric Processing of Nitrophenols and Nitrocresols from Biomass Burning
1192 Emissions, *J. Geophys. Res. Atmos.*, 0–3, doi:10.1029/2020JD033401, 2020a.

1193 Wang, M., Chen, D., Xiao, M., Ye, Q., Stolzenburg, D., Hofbauer, V., Ye, P., Vogel,

1194 A. L., Mauldin, R. L., Amorim, A., Baccharini, A., Baumgartner, B., Brilke, S., Dada,
1195 L., Dias, A., Duplissy, J., Finkenzeller, H., Garmash, O., He, X.-C., Hoyle, C. R.,
1196 Kim, C., Kvashnin, A., Lehtipalo, K., Fischer, L., Molteni, U., Petäjä, T., Pospisilova,
1197 V., Quéléver, L. L. J., Rissanen, M., Simon, M., Tauber, C., Tomé, A., Wagner, A. C.,
1198 Weitz, L., Volkamer, R., Winkler, P. M., Kirkby, J., Worsnop, D. R., Kulmala, M.,
1199 Baltensperger, U., Dommen, J., El-Haddad, I. and Donahue, N. M.: Photo-oxidation
1200 of Aromatic Hydrocarbons Produces Low-Volatility Organic Compounds, *Environ.*
1201 *Sci. Technol.*, 54(13), 7911–7921, doi:10.1021/acs.est.0c02100, 2020b.

1202 Wang, Q., He, X., Zhou, M., Huang, D. D., Qiao, L., Zhu, S., Ma, Y., Wang, H., Li,
1203 L., Huang, C., Huang, X. H. H., Xu, W., Worsnop, D., Goldstein, A. H., Guo, H. and
1204 Yu, J. Z.: Hourly Measurements of Organic Molecular Markers in Urban Shanghai,
1205 China: Primary Organic Aerosol Source Identification and Observation of Cooking
1206 Aerosol Aging, *ACS Earth Sp. Chem.*, 4(9), 1670–1685,
1207 doi:10.1021/acsearthspacechem.0c00205, 2020c.

1208 Wang, T., Tham, Y. J., Xue, L., Li, Q., Zha, Q., Wang, Z., Poon, S. C. N., Dube, W.
1209 P., Blake, D. R., Louie, P. K. K., Luk, C. W. Y., Tsui, W., Brown, S. S., Osthoff, H.
1210 D., Roberts, J. M., Ravishankara, A. R., Williams, E. J., Lerner, B. M., Sommariva,
1211 R., Bates, T. S., Coffman, D., Quinn, P. K., Dibb, J. E., Stark, H., Burkholder, J. B.,
1212 Talukdar, R. K., Meagher, J., Fehsenfeld, F. C. and Brown, S. S.: Observations of
1213 nitryl chloride and modeling its source and effect on ozone in the planetary boundary
1214 layer of southern China, *J. Geophys. Res.*, 121(5), 2476–2489,
1215 doi:10.1002/2015JD024556, 2016.

1216 Wang, X., Jacob, D. J., Eastham, S. D., Sulprizio, M. P., Zhu, L., Chen, Q.,
1217 Alexander, B., Sherwen, T., Evans, M. J., Lee, B. H., Haskins, J. D., Lopez-Hilfiker,
1218 F. D., Thornton, J. A., Huey, G. L. and Liao, H.: The role of chlorine in global
1219 tropospheric chemistry, *Atmos. Chem. Phys.*, 19(6), 3981–4003, doi:10.5194/acp-19-
1220 3981-2019, 2019.

1221 Wang, Z., Yuan, B., Ye, C., Roberts, J., Wisthaler, A., Lin, Y., Li, T., Wu, C., Peng,
1222 Y., Wang, C., Wang, S., Yang, S., Wang, B., Qi, J., Wang, C., Song, W., Hu, W.,
1223 Wang, X., Xu, W., Ma, N., Kuang, Y., Tao, J., Zhang, Z., Su, H., Cheng, Y., Wang,

1224 X. and Shao, M.: High Concentrations of Atmospheric Isocyanic Acid (HNCO)
1225 Produced from Secondary Sources in China, *Environ. Sci. Technol.*, 11818–11826,
1226 doi:10.1021/acs.est.0c02843, 2020d.

1227 Wennberg, P. O., Bates, K. H., Crouse, J. D., Dodson, L. G., McVay, R. C., Mertens,
1228 L. A., Nguyen, T. B., Praske, E., Schwantes, R. H., Smarte, M. D., St Clair, J. M.,
1229 Teng, A. P., Zhang, X. and Seinfeld, J. H.: Gas-Phase Reactions of Isoprene and Its
1230 Major Oxidation Products, *Chem. Rev.*, 118(7), 3337–3390,
1231 doi:10.1021/acs.chemrev.7b00439, 2018.

1232 Wu, C., Wang, C., Wang, S., Wang, W., Yuan, B., Qi, J., Wang, B., Wang, H., Wang,
1233 C., Song, W., Wang, X., Hu, W., Lou, S., Ye, C., Peng, Y., Wang, Z., Huangfu, Y.,
1234 Xie, Y., Zhu, M., Zheng, J., Wang, X., Jiang, B., Zhang, Z. and Shao, M.:
1235 Measurement report: Important contributions of oxygenated compounds to emissions
1236 and chemistry of VOCs in urban air, *Atmos. Chem. Phys.*, 14769–14785,
1237 doi:10.5194/acp-2020-152, 2020.

1238 Xiong, F., McAvey, K. M., Pratt, K. A., Groff, C. J., Hostetler, M. A., Lipton, M. A.,
1239 Starn, T. K., Seeley, J. V, Bertman, S. B. and Teng, A. P.: Observation of Isoprene
1240 Hydroxynitrates in the Southeastern United States and Implications for the Fate of
1241 NO_x, *Atmos. Chem. Phys.*, 15, 11257, 2015.

1242 Xue, L., Gu, R., Wang, T., Wang, X., Saunders, S., Blake, D., Louie, P. K. K., Luk,
1243 C. W. Y., Simpson, I., Xu, Z., Wang, Z., Gao, Y., Lee, S., Mellouki, A. and Wang,
1244 W.: Oxidative capacity and radical chemistry in the polluted atmosphere of Hong
1245 Kong and Pearl River Delta region: analysis of a severe photochemical smog episode,
1246 *Atmos. Chem. Phys.*, 16(15), 9891–9903, doi:10.5194/acp-16-9891-2016, 2016.

1247 Yang, Y., Shao, M., Wang, X., Nölscher, A. C., Kessel, S., Guenther, A. and
1248 Williams, J.: Towards a quantitative understanding of total OH reactivity: A review,
1249 *Atmos. Environ.*, 134(2), 147–161, doi:10.1016/j.atmosenv.2016.03.010, 2016.

1250 Yang, Y., Shao, M., Keßel, S., Li, Y., Lu, K., Lu, S., Williams, J., Zhang, Y., Zeng,
1251 L., Nölscher, A. C., Wu, Y., Wang, X. and Zheng, J.: How the OH reactivity affects
1252 the ozone production efficiency: case studies in Beijing and Heshan, China, *Atmos.*
1253 *Chem. Phys.*, 17(11), 7127–7142, doi:10.5194/acp-17-7127-2017, 2017.

1254 Yasmeen, F., Szmigielski, R., Vermeulen, R., Gomez-Gonzalez, Y., Surratt, J. D.,
1255 Chan, A. W. H., Seinfeld, J. H., Maenhaut, W. and Claeys, M.: Mass spectrometric
1256 characterization of isomeric terpenoic acids from the oxidation of alpha-pinene, beta-
1257 pinene, d-limonene, and Delta(3)-carene in fine forest aerosol, *J. MASS Spectrom.*,
1258 46(4), 425–442, doi:10.1002/jms.1911, 2011.

1259 Yatavelli, R. L. N., Lopez-Hilfiker, F., Wargo, J. D., Kimmel, J. R., Cubison, M. J.,
1260 Bertram, T. H., Jimenez, J. L., Gonin, M., Worsnop, D. R. and Thornton, J. A.: A
1261 Chemical Ionization High-Resolution Time-of-Flight Mass Spectrometer Coupled to a
1262 Micro Orifice Volatilization Impactor (MOVI-HRToF-CIMS) for Analysis of Gas and
1263 Particle-Phase Organic Species, *Aerosol Sci. Technol.*, 46(12), 1313–1327,
1264 doi:10.1080/02786826.2012.712236, 2012.

1265 Yuan, B., Veres, P. R., Warneke, C., Roberts, J. M., Gilman, J. B., Koss, A., Edwards,
1266 P. M., Graus, M., Kuster, W. C., Li, S. M., Wild, R. J., Brown, S. S., Dubé, W. P.,
1267 Lerner, B. M., Williams, E. J., Johnson, J. E., Quinn, P. K., Bates, T. S., Lefer, B.,
1268 Hayes, P. L., Jimenez, J. L., Weber, R. J., Zamora, R., Ervens, B., Millet, D. B.,
1269 Rappenglück, B. and De Gouw, J. A.: Investigation of secondary formation of formic
1270 acid: Urban environment vs. oil and gas producing region, *Atmos. Chem. Phys.*,
1271 15(4), 1975–1993, doi:10.5194/acp-15-1975-2015, 2015.

1272 Yuan, B., Liggio, J., Wentzell, J., Li, S. M., Stark, H., Roberts, J. M., Gilman, J.,
1273 Lerner, B., Warneke, C., Li, R., Leithead, A., Osthoff, H. D., Wild, R., Brown, S. S.
1274 and De Gouw, J. A.: Secondary formation of nitrated phenols: Insights from
1275 observations during the Uintah Basin Winter Ozone Study (UBWOS) 2014, *Atmos.*
1276 *Chem. Phys.*, 16(4), 2139–2153, doi:10.5194/acp-16-2139-2016, 2016.

1277 Yuan, B., Koss, A. R., Warneke, C., Coggon, M., Sekimoto, K. and De Gouw, J. A.:
1278 Proton-Transfer-Reaction Mass Spectrometry: Applications in Atmospheric Sciences,
1279 *Chem. Rev.*, 117(21), 13187–13229, doi:10.1021/acs.chemrev.7b00325, 2017.

1280 Zhang, Q., Yuan, B., Shao, M., Wang, X., Lu, S., Lu, K., Wang, M., Chen, L., Chang,
1281 C.-C. and Liu, S. C.: Variations of ground-level O₃ and its precursors in Beijing in
1282 summertime between 2005 and 2011, *Atmos. Chem. Phys.*, 14(12), 6089–6101,
1283 doi:10.5194/acp-14-6089-2014, 2014.

1284 Zhang, Y. J., Tang, L. L., Wang, Z., Yu, H. X., Sun, Y. L., Liu, D., Qin, W.,
1285 Canonaco, F., Prévôt, A. S. H., Zhang, H. L. and Zhou, H. C.: Insights into
1286 characteristics, sources, and evolution of submicron aerosols during harvest seasons in
1287 the Yangtze River delta region, China, *Atmos. Chem. Phys.*, 15(3), 1331–1349,
1288 doi:10.5194/acp-15-1331-2015, 2015.

1289 Zhao, R.: *The Recent Development and Application of Chemical Ionization Mass*
1290 *Spectrometry in Atmospheric Chemistry.*, 2018.

1291 Zhao, Y., Nguyen, N. T., Presto, A. A., Hennigan, C. J., May, A. A. and Robinson, A.
1292 L.: Intermediate Volatility Organic Compound Emissions from On-Road Gasoline
1293 Vehicles and Small Off-Road Gasoline Engines, *Environ. Sci. Technol.*, 50(8), 4554–
1294 4563, doi:10.1021/acs.est.5b06247, 2016.

1295 Zhou, Y., Huang, X. H., Bian, Q., Griffith, S. M., Louie, P. K. K. and Yu, J. Z.:
1296 Sources and atmospheric processes impacting oxalate at a suburban coastal site in
1297 Hong Kong: Insights inferred from 1 year hourly measurements, *J. Geophys. Res.*
1298 *Atmos.*, 120(18), 9772–9788, doi:10.1002/2015JD023531, 2015.

1299

1300 **Table 1.** The detected ions discussed in the text.

Ion formula	m/z	Assigned compounds	Possible formation pathways	References
$C_6H_{10}O_5I^-$	288.96	Levoglucozan, mannosan and galactosan	Biomass burning or cooking emissions	(Gaston et al., 2016; Reyes-Villegas et al., 2018)
$C_6H_{12}O_5I^-$	290.97	Fucose	Biomass burning emissions	(Qi et al., 2019)
$C_6H_5NO_3I^-$	265.93	Nitro-phenols	Direct emissions, oxidation of aromatics in the presence of NO _x	(Gaston et al., 2016; Yuan et al., 2016)
$C_6H_5NO_4I^-$	281.93	Nitro-benzenediols	Direct emissions, oxidation of aromatics in the presence of NO _x	(Gaston et al., 2016; Yuan et al., 2016)
$C_6H_4N_2O_5I^-$	310.92	Dinitro-phenols	Direct emissions, oxidation of aromatics in the presence of NO _x	(Gaston et al., 2016; Yuan et al., 2016)
$C_7H_7NO_3I^-$	279.95	Methyl nitro-phenols	Direct emissions, oxidation of aromatics in the presence of NO _x	(Gaston et al., 2016; Yuan et al., 2016)
$C_7H_7NO_4I^-$	295.94	Methyl nitro-benzenediols	Direct emissions, oxidation of aromatics in the presence of NO _x	(Gaston et al., 2016; Yuan et al., 2016)
$C_7H_6O_4I^-$	280.93	Dihydroxy methyl benzoquinone	Aromatics + OH	(Schwantes et al., 2017; Wang et al., 2020b)
$C_7H_8O_4I^-$	282.95	Tetrahydroxy toluene	Aromatics + OH	(Schwantes et al., 2017; Wang et al., 2020b)
$C_7H_8O_5I^-$	298.94	Pentahydroxy toluene, fragments of C9 aromatics	Aromatics + OH	(Mehra et al., 2020; Schwantes et al., 2017)

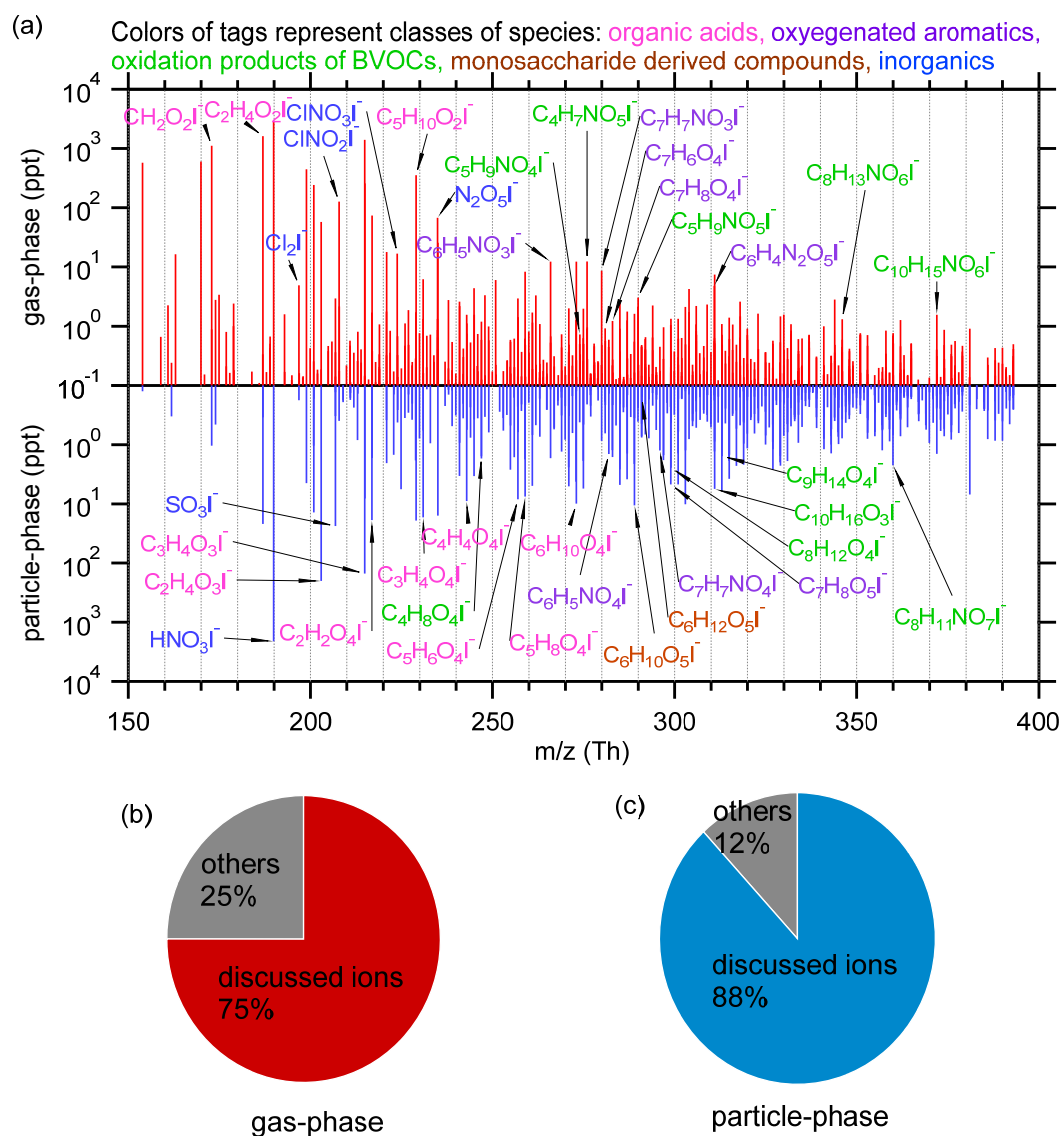
$CH_2O_2I^-$	172.91	Formic acid	Oxidation of VOCs	(Lee et al., 2014; Yuan et al., 2015)
$C_2H_4O_2I^-$	186.93	Acetic acid	Oxidation of VOCs	(Lee et al., 2014; Mattila et al., 2018)
$C_5H_{10}O_2I^-$	228.97	Pentanoic acid	Traffic emissions, secondary formation	(Mattila et al., 2018)
$C_2H_4O_3I^-$	202.92	Glycolic acid	Oxidation of VOCs	(Lee et al., 2014; Lim et al., 2005)
$C_3H_4O_3I^-$	214.92	Pyruvic acid	Photolysis of methylglyoxal, BVOCs+OH, photo-oxidation of aromatics in the presence of NO _x	(Eger et al., 2020; Mattila et al., 2018)
$C_2H_2O_4I^-$	216.90	Oxalic acid	Aqueous-phase photooxidation of glyoxal, photo-oxidation of VOCs	(Carlton et al., 2007; Lee et al., 2014; Zhou et al., 2015)
$C_3H_4O_4I^-$	230.92	Malonic acid, hydroxypyruvic acid	Oxidation of VOCs	(Kawamura and Bikkina, 2016; Lee et al., 2014)
$C_4H_4O_4I^-$	242.92	Maleic acid, fumaric acid	Oxidation of aromatics	(Brege et al., 2018; Kawamura et al., 1996)
$C_5H_6O_4I^-$	256.93	Unsaturated dicarboxylic acid	Oxidation of aromatics	(Brege et al., 2018; Kawamura et al., 1996)
$C_5H_8O_4I^-$	258.95		Photo-oxidation of VOCs	(Berndt et al., 2019; Kawamura and Bikkina, 2016)
$C_6H_{10}O_4I^-$	272.96		Photo-oxidation of VOCs	(Berndt et al., 2019; Kawamura and Bikkina, 2016)

$C_4H_8O_4I^-$	246.95	2-methylglyceric acid	Isoprene SOA component under high NO _x conditions	(Surratt et al., 2006, 2010)
$C_5H_9NO_4I^-$	273.96	IHN (isoprene hydroxy nitrates)	1st-generation organic nitrates from reaction: isoprene+OH+NO _x , isoprene+NO ₃	(Jacobs et al., 2014; Xiong et al., 2015)
$C_4H_7NO_5I^-$	275.94	MVKN/MACRN	2nd-generation organic nitrates from oxidation of IHN in the presence of NO _x	(Fisher et al., 2016; Paulot et al., 2009)
$C_5H_9NO_5I^-$	289.95	C5 nitrooxy hydroperoxide, C5 nitrooxy hydroxyepoxide, C5 dihydroxy nitrate	isoprene+NO ₃ , isoprene+OH+NO _x	(Ng et al., 2017; Schwantes et al., 2015; Wennberg et al., 2018)
$C_8H_{12}O_4I^-$	298.98	Dicarboxylic and oxocarboxylic acids like norpinic acid, terpenylic acid	Monoterpenes+OH, monoterpenes O ₃	(Fang et al., 2017; Mutzel et al., 2016; Yasmeen et al., 2011)
$C_9H_{14}O_4I^-$	312.99	Dicarboxylic and oxocarboxylic acids like pinic acid, homoterpenylic acid, caric acid	Monoterpenes+OH, monoterpenes O ₃	(Fang et al., 2017; Mutzel et al., 2016; Yasmeen et al., 2011)
$C_{10}H_{16}O_3I^-$	311.02	Oxocarboxylic acids like	Monoterpenes+OH, monoterpenes O ₃	(Fang et al., 2017; Glasius et al.,

		pinonic acid, caronic acid		2000; Yasmeen et al., 2011)
$C_8H_{13}NO_6I^-$	345.98	Organic nitrates from monoterpenes	Monoterpenes+OH+NO _x , monoterpenes +NO ₃	(Lee et al., 2016; Nah et al., 2016)
$C_8H_{11}NO_7I^-$	359.96	Organic nitrates from monoterpenes	Monoterpenes+OH+NO _x , monoterpenes O ₃ +NO ₃	(Carslaw, 2013; Lee et al., 2016)
$C_{10}H_{15}NO_6I^-$	372.00	Organic nitrates from monoterpenes, peroxyacetyl nitrate from pinonaldehyde	Monoterpenes+OH+NO _x , monoterpenes O ₃ +NO ₃	(Boyd et al., 2015; Massoli et al., 2018; Schwantes et al., 2020)
HSO_4^-	96.96	Sulfuric acid	Oxidation of SO ₂ etc.	(Le Breton et al., 2018b)
SO_3I^-	206.86	Sulfur trioxide, Fragment of organosulfates	Oxidation of SO ₂ , decomposition of organosulfates	(Surratt et al., 2007)
$C_2H_3SO_6^-$	154.96	Glycolic acid sulfate	Aqueous reaction of glycolic acid and sulfuric acid	(Galloway et al., 2009; Huang et al., 2018)
$CH_3SO_3^-$	94.98	Methanesulfon ic acid	Oxidation of dimethyl sulfide	(Chen and Finlayson-Pitts, 2017; Gondwe et al., 2003)
$N_2O_5I^-$	234.89	Dinitrogen pentoxide	NO ₃ + NO ₂ + M	(Le Breton et al., 2018a; Wang et al., 2016)
$ClNO_2I^-$	207.87	Nitryl chloride	N ₂ O ₅ (g) + Cl ⁻ (aq)	(Le Breton et al., 2018a; Wang et al., 2016)

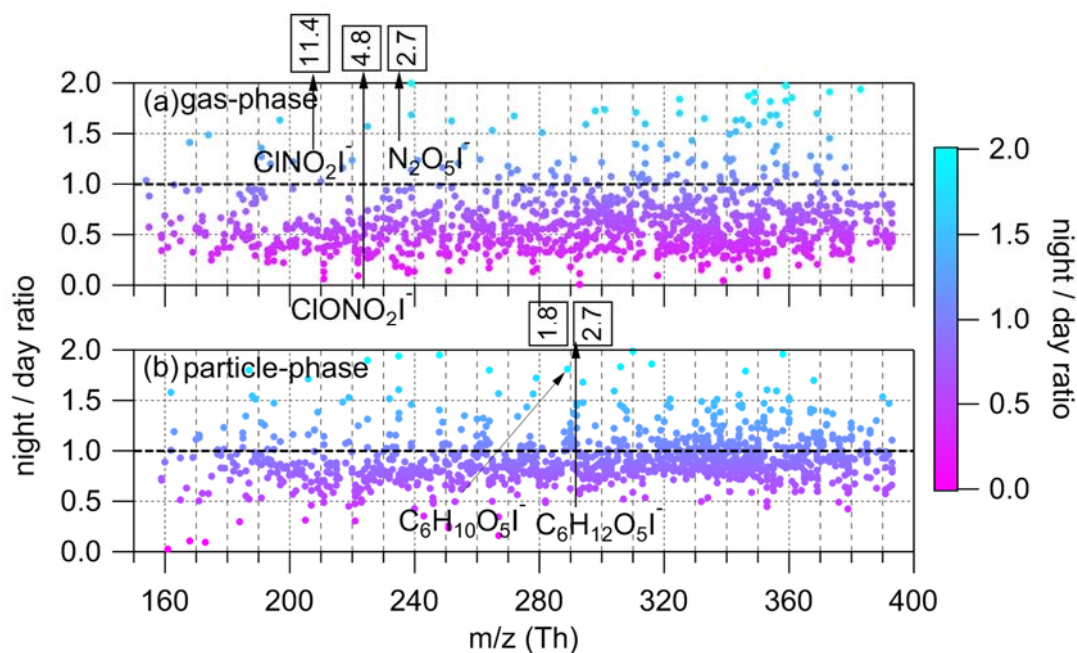
$ClNO_3I^-$	223.86	Chlorine nitrate	$ClO + NO_2 + M$	(Liu et al., 2017; Sander and Crutzen, 1996)
Cl_2I^-	196.84	Chlorine	Heterogeneous reactions of Cl^- and reactive chlorine like HOCl, $ClNO_2$ etc.	(Le Breton et al., 2018a; Liu et al., 2017; Wang et al., 2019)
HNO_3I^-	189.90	Nitric acid	$NO_x + OH$, hydrolysis of organic nitrates and N_2O_5	(Fisher et al., 2016; Wang et al., 2016)

1301



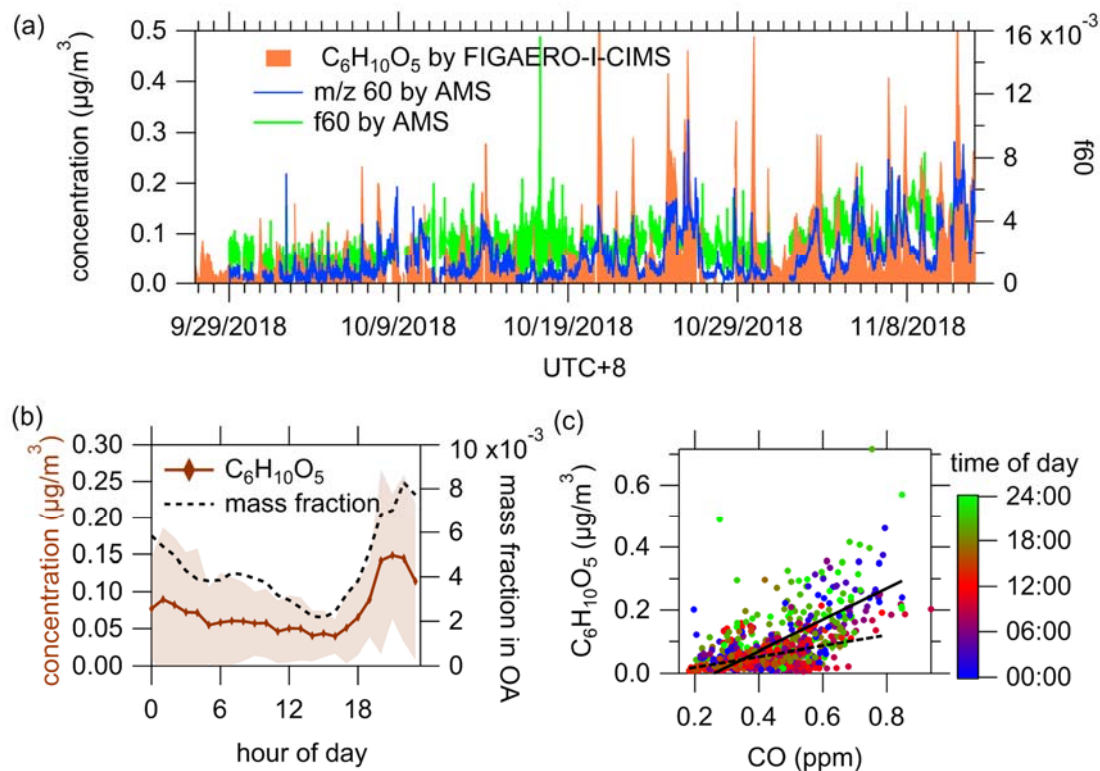
1303

1304 **Figure 1.** (a) Mass spectra of iodide charged ion within m/z 150-400 Th in gas-phase
 1305 (red) and particle-phase (blue), respectively. (b and c) The fractions of I-adduct ions
 1306 discussed in the main text (Table 1) in the total ion signals for I-adduct ions measured
 1307 in gas-phase (b) and particle-phase (c), respectively.



1309

1310 **Figure 2.** The ratios of concentrations at night (10 pm - 6 am) to concentrations during
1311 the day (10 am - 6 pm) for ions ranging from 150 to 400 Th in gas-phase (a) and particle-
1312 phase (b). The range of y-axis is set between 0 and 2 for clarity, although the ratios of
1313 some compounds are larger than 2. The numbers in boxes indicate the night/day ratios
1314 of tagged ions that exceed the y-axis ranges.



1315

1316

1317

1318

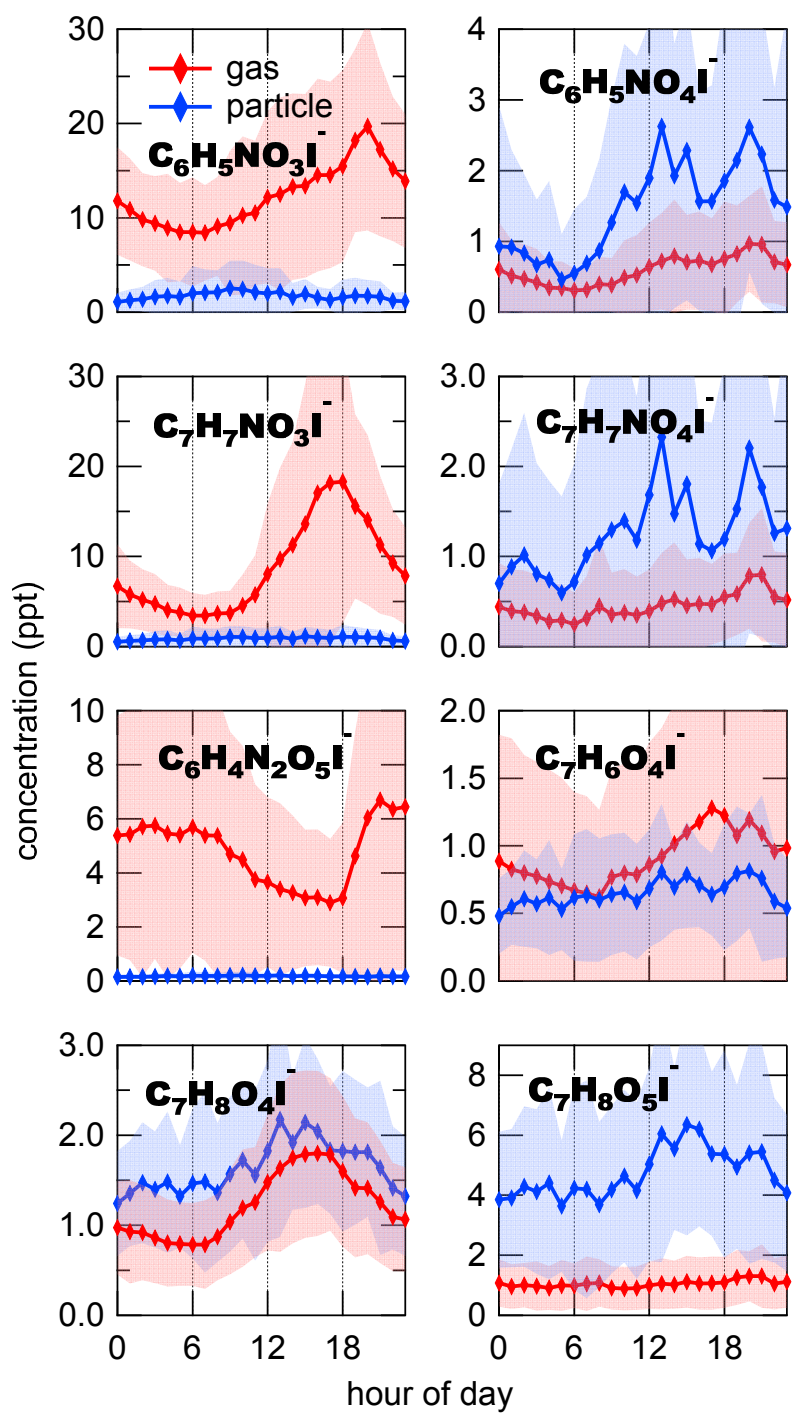
1319

1320

1321

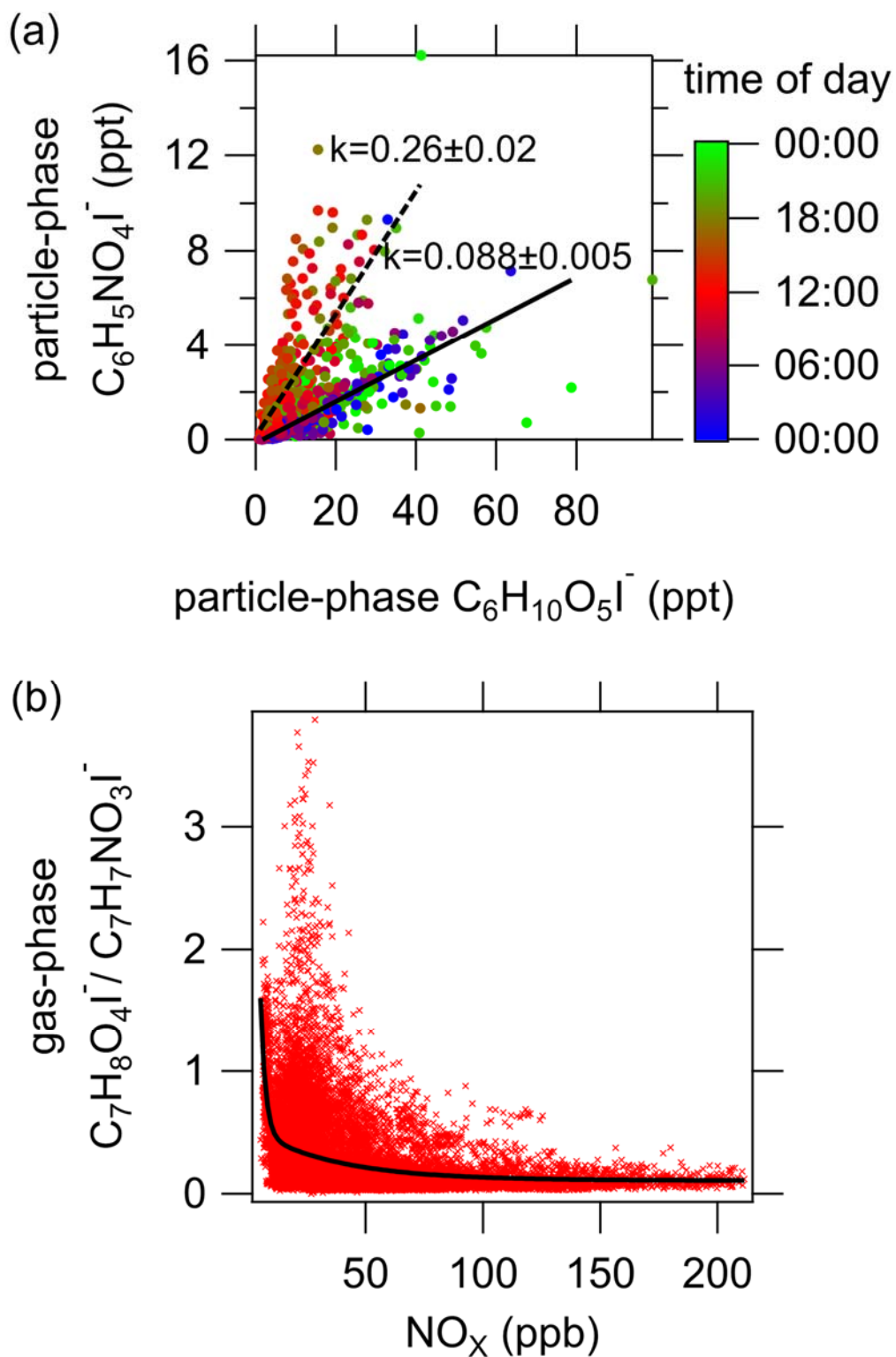
1322

Figure 3. (a) Time series of particulate $C_6H_{10}O_5$ measured by FIGAERO-I-CIMS, m/z 60 fragment and f60 measured by AMS. Background f60=0.3% and background m/z 60=0.3% \times OA were subtracted from f60 and m/z 60 (Cubison et al., 2011; Hu et al., 2016). (b) Diurnal variations of particulate $C_6H_{10}O_5$ and its mass fraction in OA. (c) Correlation between CO and particulate $C_6H_{10}O_5$. The dash and solid lines indicate the ratios during daytime (10 am - 6 pm, $0.17\pm 0.02 \mu g \cdot m^{-3}/ppm$) and nighttime (10 pm - 6 am, $0.50\pm 0.03 \mu g \cdot m^{-3}/ppm$), respectively.



1323

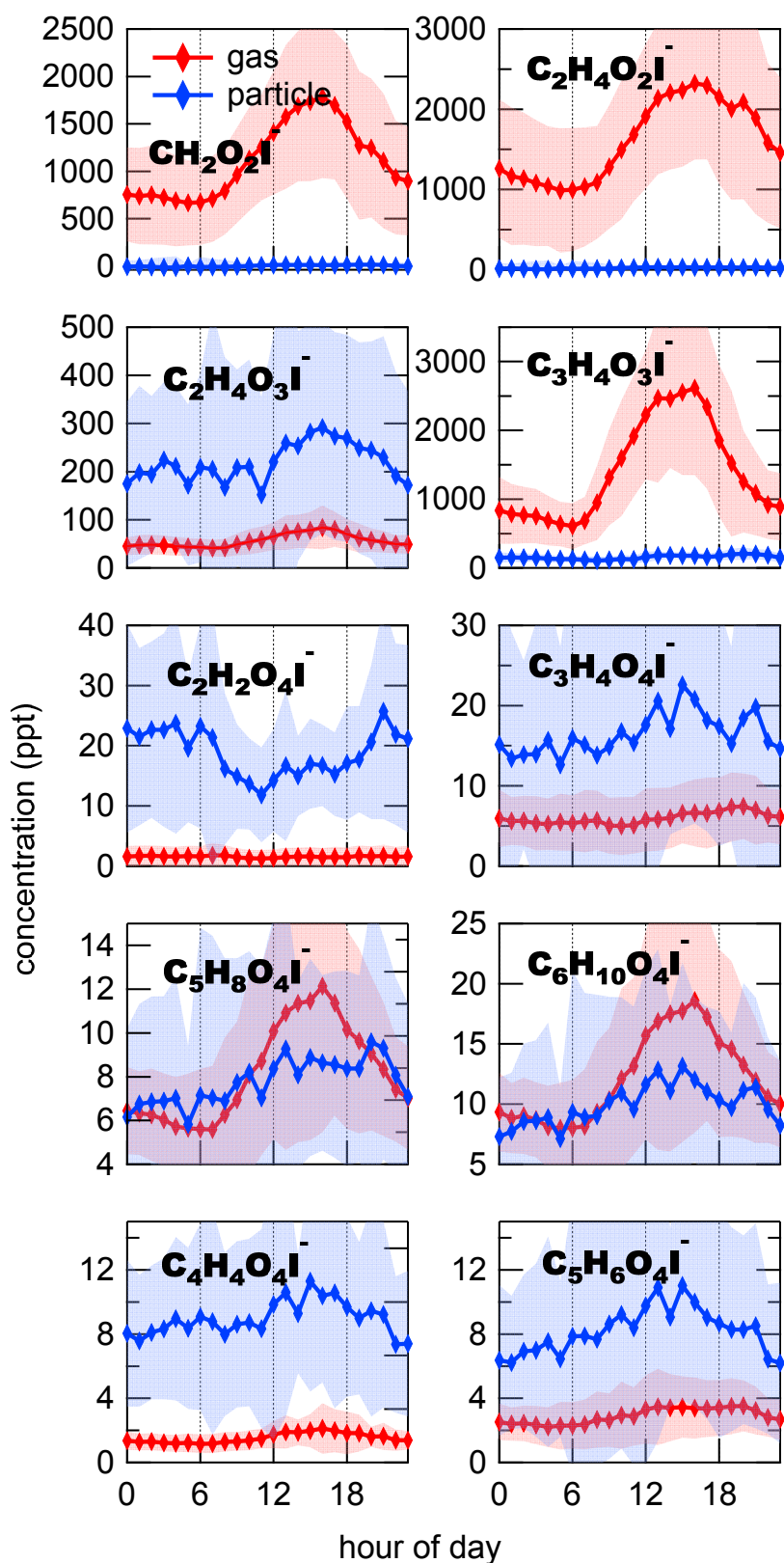
1324 **Figure 4.** Diurnal variations of oxidized aromatics including nitro-phenols
 1325 ($C_6H_5NO_3I^-$), nitro-benzenediols ($C_6H_5NO_4I^-$), methyl nitro-phenols ($C_7H_7NO_3I^-$),
 1326 methyl nitro-benzenediols ($C_7H_7NO_4I^-$), dinitro-phenols ($C_6H_4N_2O_5I^-$), dihydroxy
 1327 methyl benzoquinone ($C_7H_6O_4I^-$), tetrahydroxy toluene ($C_7H_8O_4I^-$), pentahydroxy
 1328 toluene and fragments of C9 aromatics ($C_7H_8O_5I^-$). The shaded areas indicate one
 1329 standard deviation.



1330

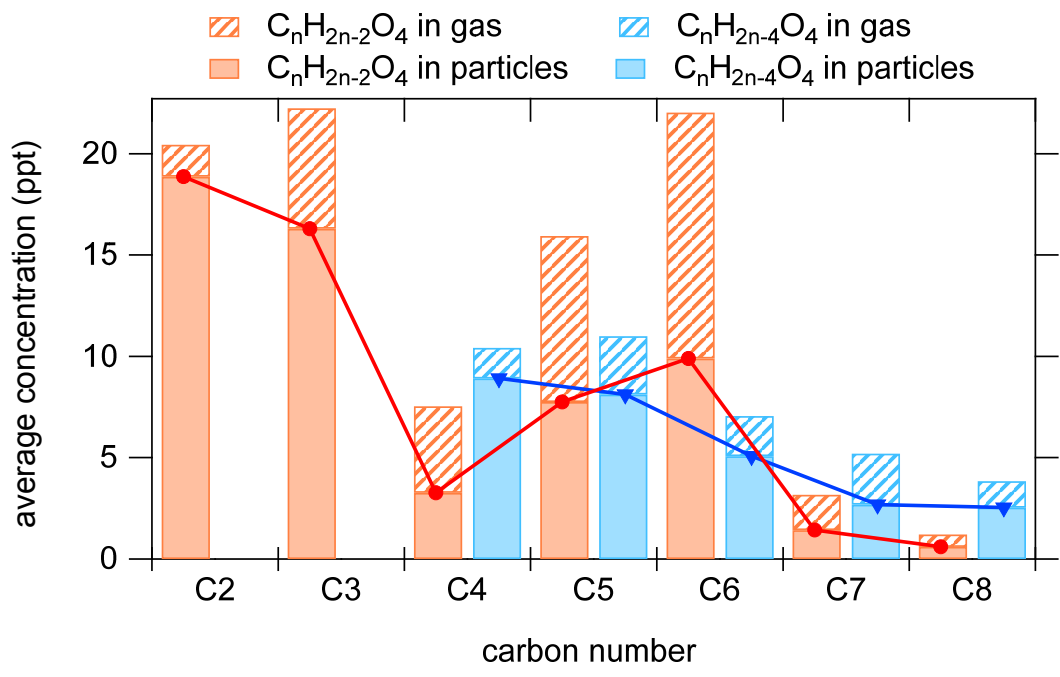
1331 **Figure 5.** (a) Correlation between particle-phase $C_6H_5NO_4I^-$ and $C_6H_{10}O_5I^-$. The
 1332 data points are color-coded using the time of the day. Solid and dash lines represent the
 1333 slopes during the nighttime and daytime, respectively. (b) Relative concentration of

1334 $C_7H_8O_4I^-$ and $C_7H_7NO_3I^-$ in the gas phase as a function of NO_x concentration. The
1335 black line is the fitted curve using a double exponential function.



1336

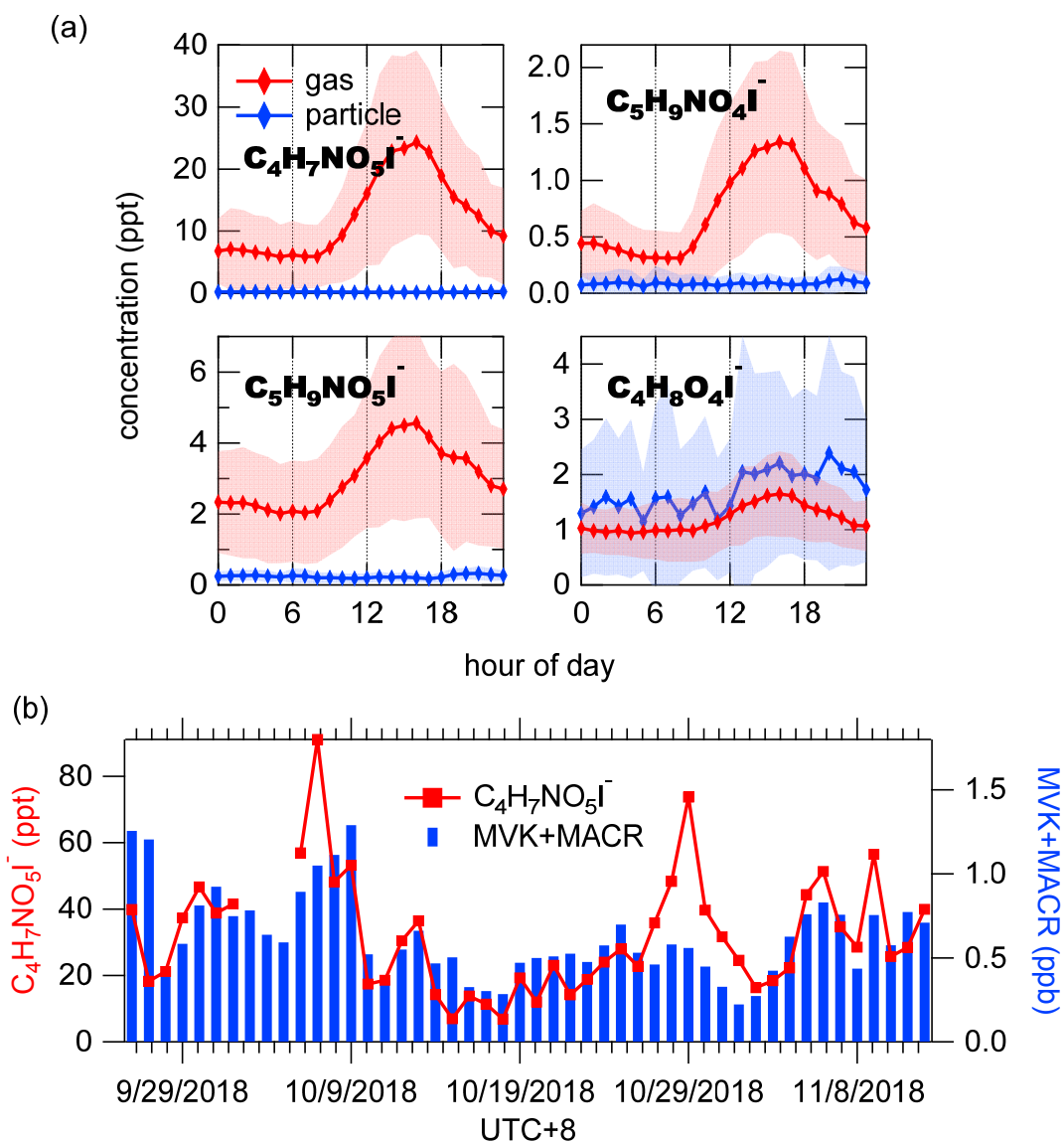
1337 **Figure 6.** Diurnal variations of organic acids in the gas phase (red) and particle phase
 1338 (blue). The shaded area indicates one standard deviation.



1339

1340 **Figure 7.** Average concentrations of compounds with the formulas of $C_nH_{2n-2}O_4$

1341 and $C_nH_{2n-4}O_4$.



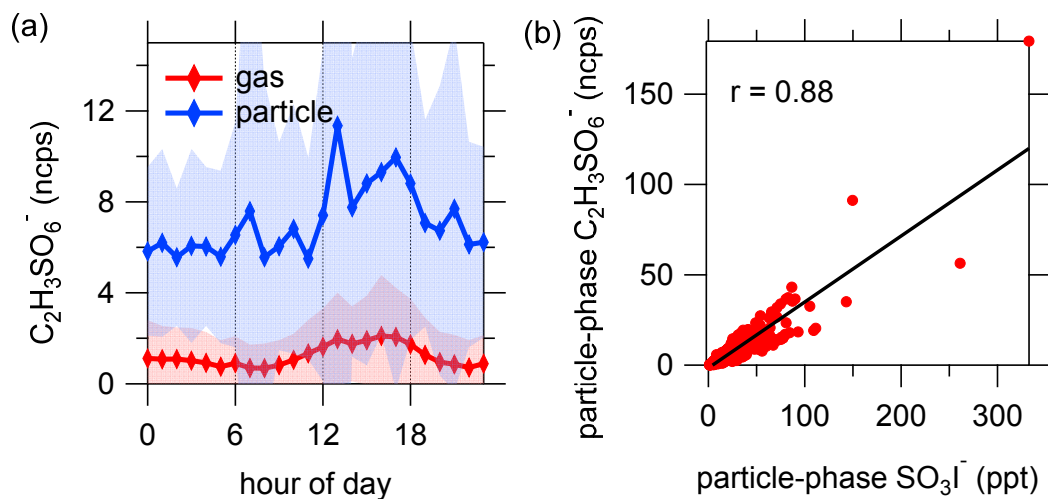
1342

1343 **Figure 8.** (a) Diurnal variations of isoprene oxidation products in the gas phase (red)

1344 and particle phase (blue). The shaded area indicates one standard deviation. (b) Time

1345 series of daily maximum concentrations of gaseous $C_4H_7NO_5I^-$ and MVK+MACR

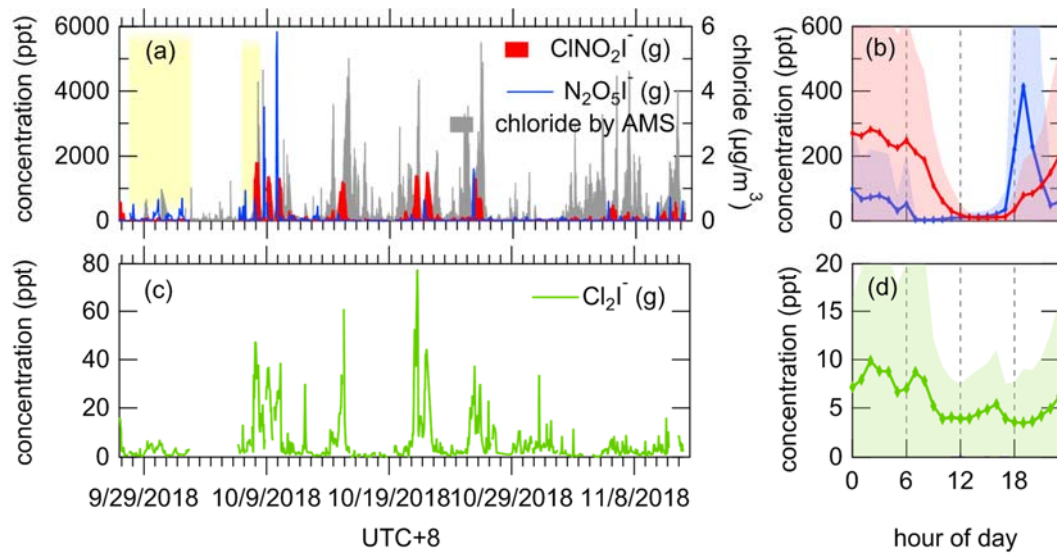
1346 ($C_4H_6OH^+$, m/z 71.05) measured by PTR-ToF-MS.



1347

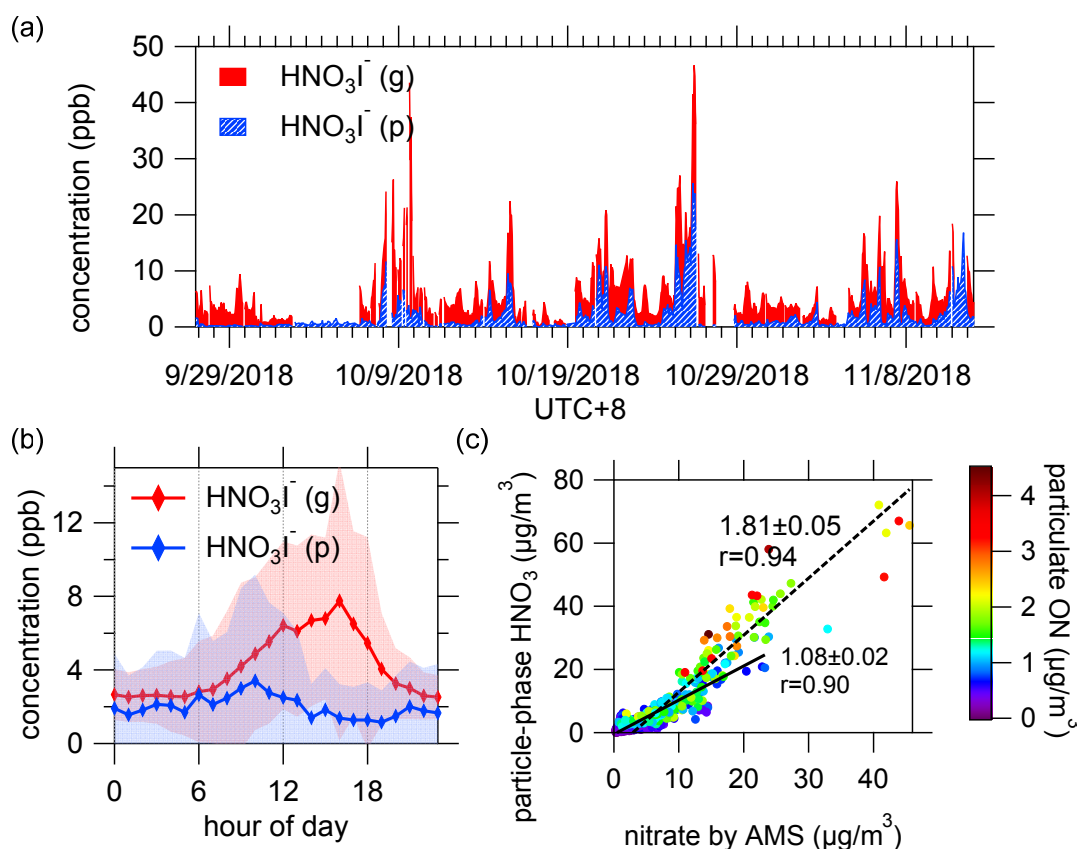
1348 **Figure 9.** (a) Diurnal variation of $C_2H_3SO_6^-$. The shaded areas indicate one standard

1349 deviation. (b) Correlation between particle-phase $C_2H_3SO_6^-$ and SO_3I^- .



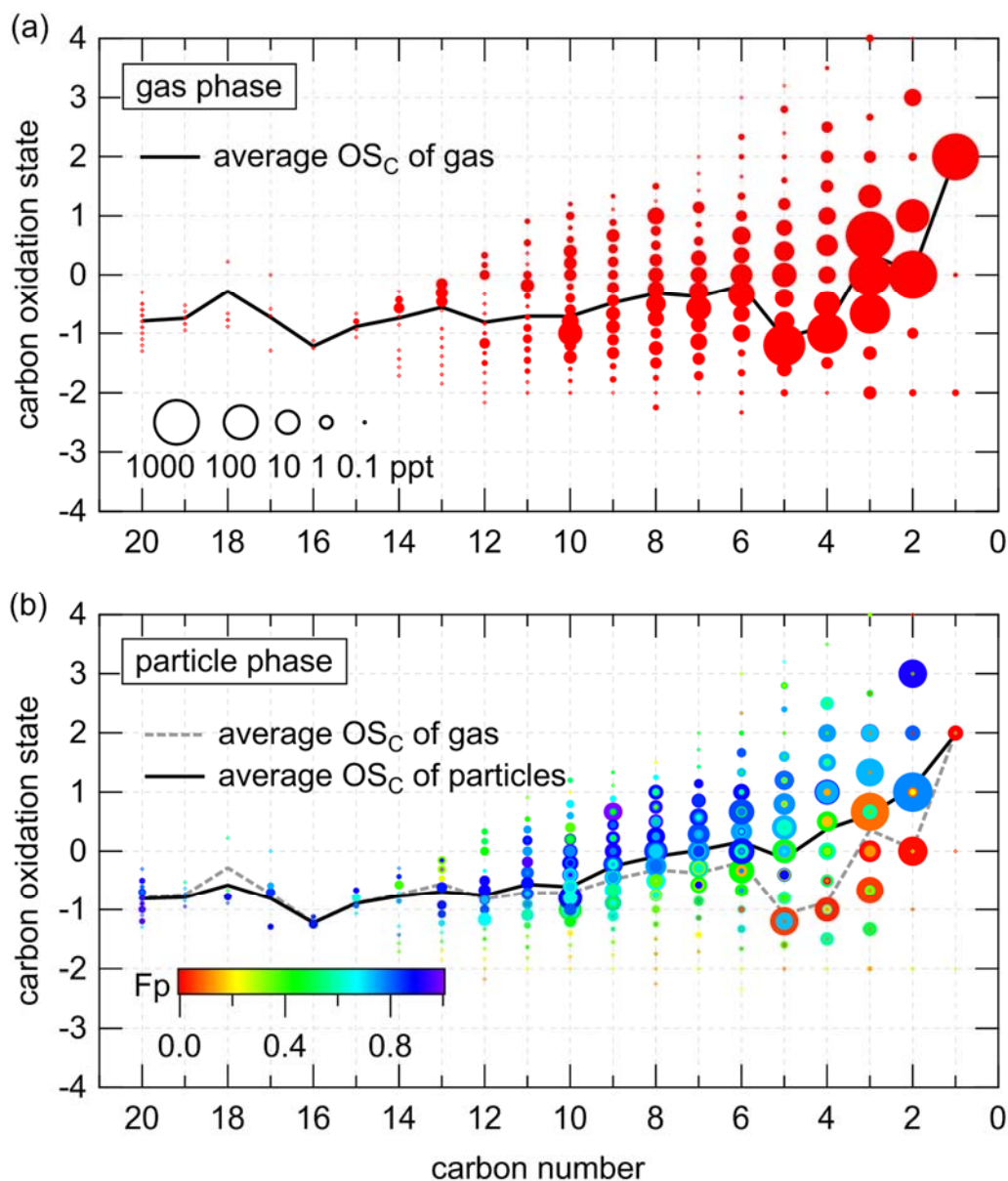
1350

1351 **Figure 10.** Time series and diurnal variations of humidity-corrected concentrations of
 1352 N_2O_5 and ClNO_2 (a, b) and Cl_2 (c, d). The tinted background indicates the days with
 1353 high concentrations of N_2O_5 but low concentrations of ClNO_2 . The shaded areas
 1354 indicate one standard deviation.



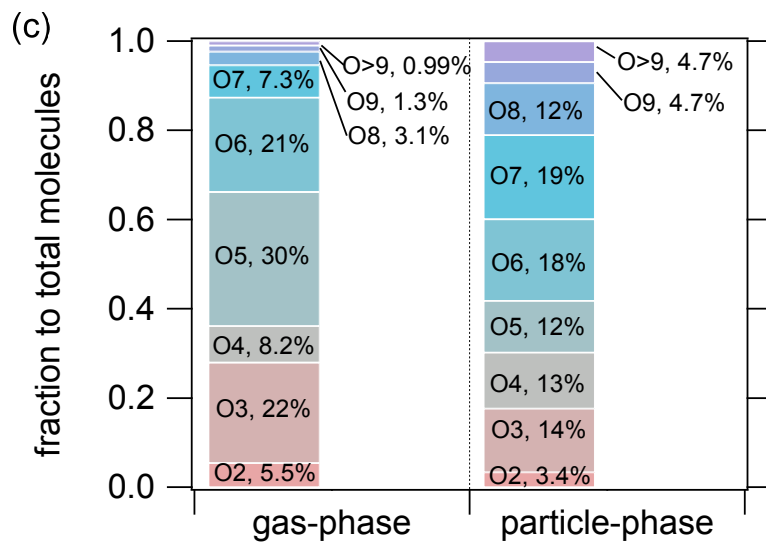
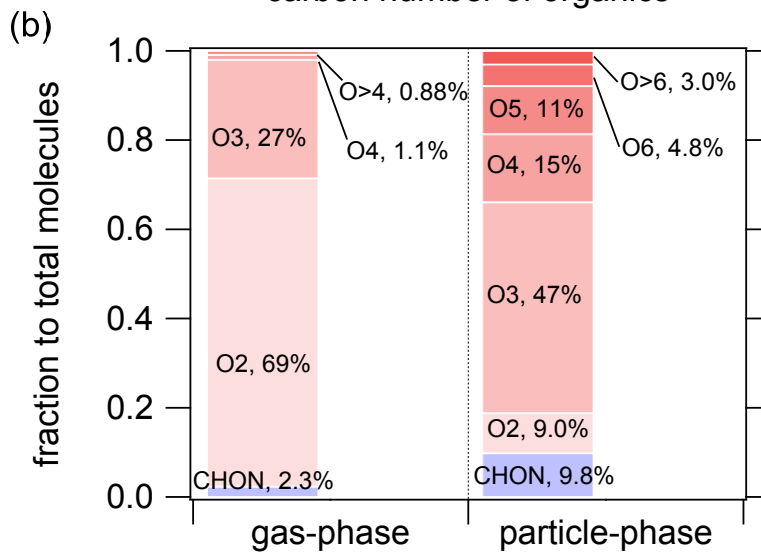
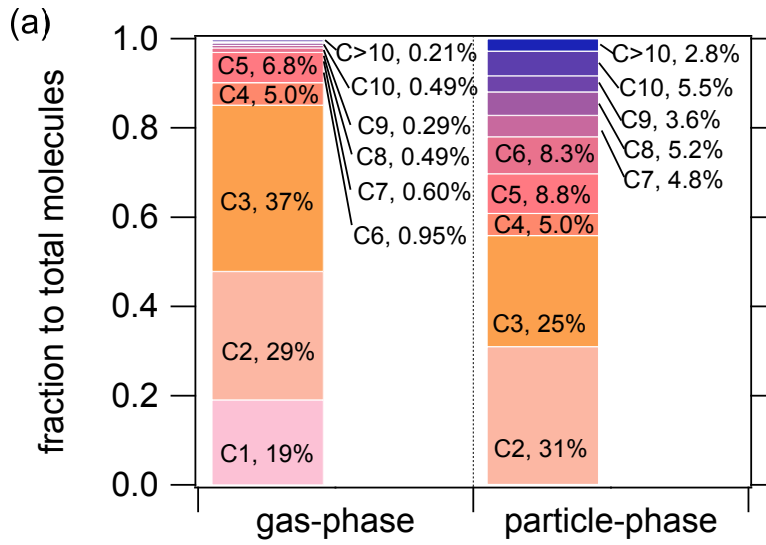
1356

1357 **Figure 11.** (a) Time series of humidity-corrected HNO_3I^- in both phases. (b) Diurnal
 1358 variation of humidity-corrected HNO_3I^- . The shaded areas indicate one standard
 1359 deviation. (c) Comparison of particle-phase HNO_3I^- and nitrate measured by AMS.
 1360 The color scale denotes particulate N-containing organic compounds measured by
 1361 FIGAERO-I-CIMS (pON). The solid and dash lines show the fitted results for the
 1362 dataset of pON less than $1 \mu\text{g}/\text{m}^3$ and more than $1 \mu\text{g}/\text{m}^3$, respectively. The
 1363 concentration of gaseous HNO_3I^- shown here only included the last 5-minute of
 1364 every gas-phase working mode, as high level of HNO_3 came out of aerosol which then
 1365 passed through the CIMS in a short time during particle analysis and a substantial
 1366 amount would subsequently accumulate on the inner surfaces, leading to a persistent
 1367 carried over signal that was long enough to disturb the next gas measurement cycle
 1368 (Palm et al., 2019).

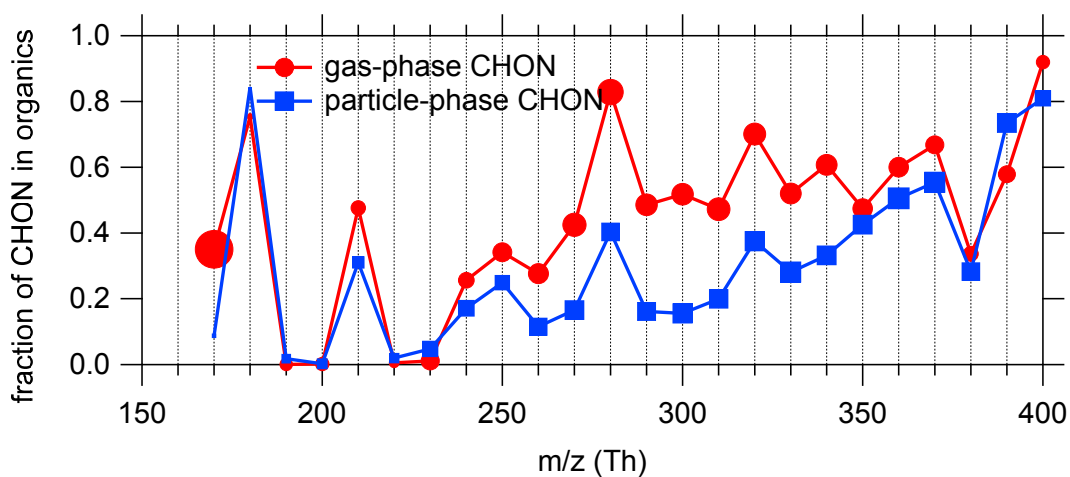


1369

1370 **Figure 12.** $\overline{OS}_C - n_C$ spaces for $C_xH_yO_z$ and $C_xH_yN_{1,2}O_z$ compounds in gas-phase
 1371 (a) and particle-phase (b). The diameters of circles are proportional to the logarithmic
 1372 average concentrations. The black lines are the average \overline{OS}_C of each carbon number
 1373 for compounds in gas-phase and particle-phase, respectively. The compounds in Fig. (b)
 1374 are color-coded by their fractions in particles.

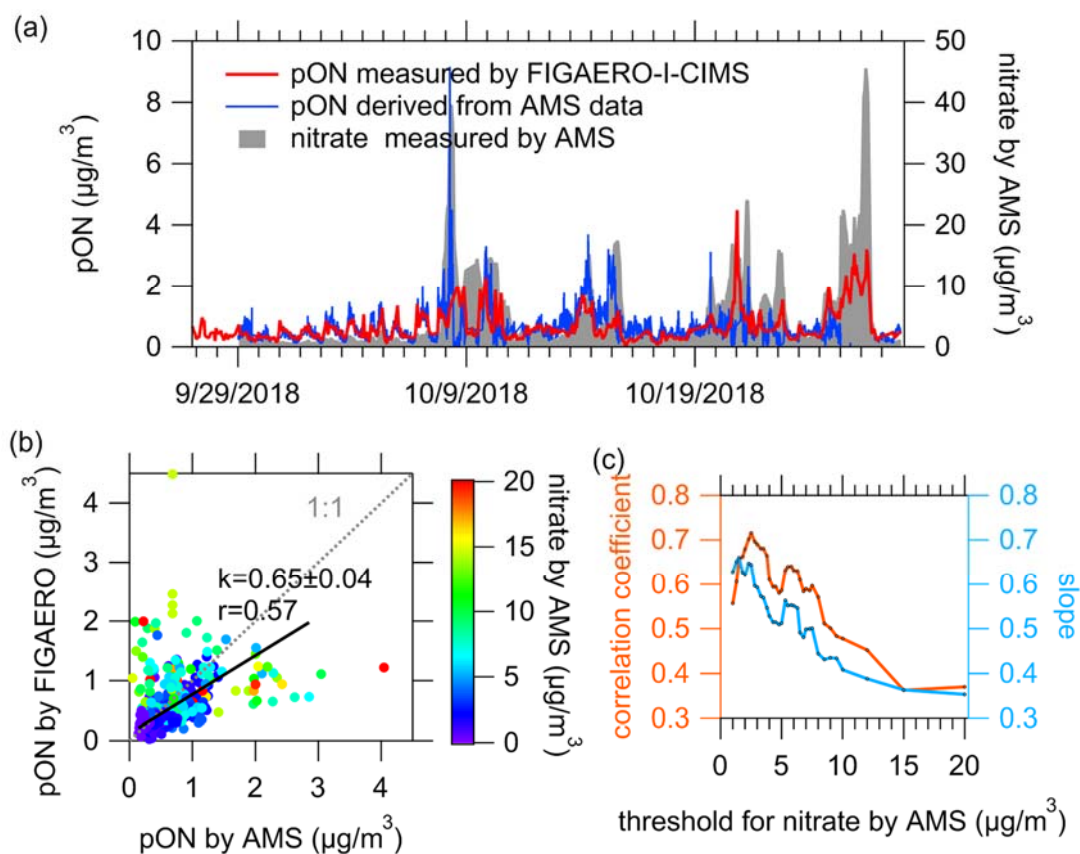


1376 **Figure 13.** Carbon number distribution (a) and oxygen number distribution of total
1377 $C_xH_yO_z$ and $C_xH_yN_{1,2}O_z$ compounds (b), and oxygen number distribution of
1378 $C_xH_yN_{1,2}O_z$ compounds (c).



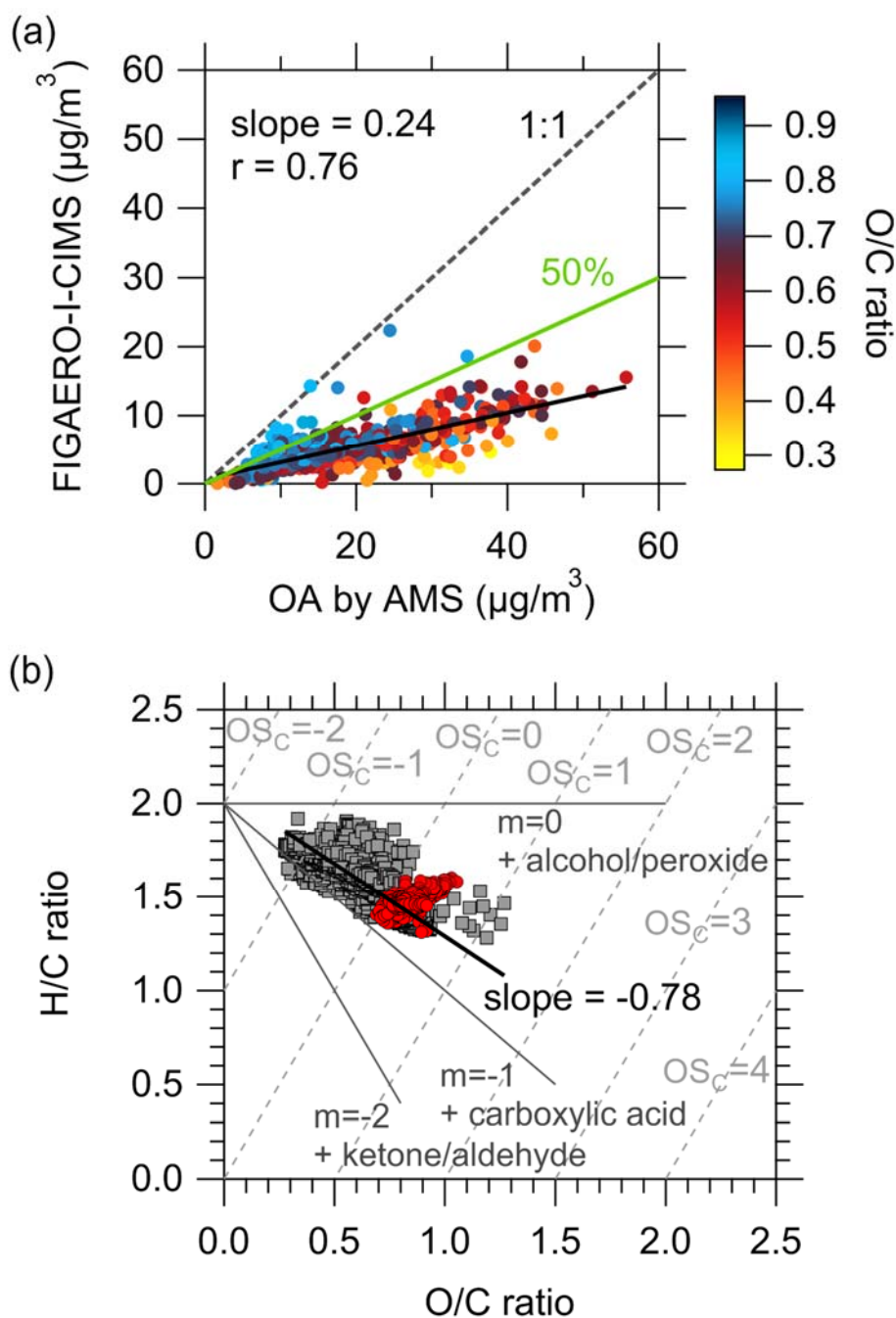
1379

1380 **Figure 14.** The average fractions of CHON to total organic compounds (CHO + CHON
 1381 + CHOS + CHONS) of every 10 Th in both phases. See Fig. S16 for the overall
 1382 distribution of the contributions of species classes to the total concentrations. Marker
 1383 sizes indicate the total concentration level in each m/z bin. High ambient concentration
 1384 of HNCO resulted in the large marker around m/z 170 in the gas phase (Wang et al.,
 1385 2020d).



1387

1388 **Figure 15.** (a) Time series of particulate N-containing organic compounds measured by
 1389 FIGAERO-I-CIMS (pON by FIGAERO), particulate organic nitrates derived from
 1390 AMS data (pON by AMS) as well as particulate inorganic nitrate. (b) Comparison of
 1391 pON by FIGAERO and pON by AMS, color-coded by the concentrations of particulate
 1392 inorganic nitrate measured by AMS. The black line presents the linear fit for nitrate by
 1393 AMS below $8 \mu\text{g}/\text{m}^3$. (c) The determined slopes and correlation coefficients between
 1394 pON by FIGAERO versus pON by AMS by filtering the data below different thresholds
 1395 of particulate inorganic nitrate measured by AMS.



1396

1397 **Figure 16.** (a) Comparison of particulate organic compounds measured by the
 1398 FIGAERO-I-CIMS and AMS, color-coded by O/C ratios measured by AMS. The black
 1399 line is the slope which represents the fraction of OA explained by the measurements of
 1400 FIGAERO-I-CIMS. The green line shows the results from previous work which were
 1401 ~50% (Lopez-Hilfiker et al., 2016; Stark et al., 2017). (b) Van Krevelen diagrams for
 1402 organic aerosol derived from AMS data (gray squares) and FIGAERO-I-CIMS data (red
 1403 circles). Black line is the slope of AMS data. Gray dotted lines are estimated carbon
 1404 oxidation state.